



Structure-activity relationships of dually-acting acetylcholinesterase inhibitors derived from tacrine on N-methyl-D-Aspartate receptors

Lukas Gorecki ^{a,1}, Anna Misiachna ^{b,c,d,1}, Jiri Damborsky ^{e,f}, Rafael Dolezal ^a, Jan Korabecny ^a, Lada Cejkova ^g, Kristina Hakenova ^g, Marketa Chvojkova ^g, Jana Zdarova Karasova ^h, Lukas Prchal ^a, Martin Novak ^{a,i}, Marharyta Kolcheva ^{b,c}, Stepan Kortus ^{b,c}, Karel Vales ^g, Martin Horak ^{b,c,*}, Ondrej Soukup ^{a,**}

^a Biomedical Research Center, University Hospital Hradec Kralove, Sokolska 581, 500 05, Hradec Kralove, Czech Republic

^b Institute of Experimental Medicine of the Czech Academy of Sciences, Videnska 1083, 14220, Prague 4, Czech Republic

^c Institute of Physiology of the Czech Academy of Sciences, Videnska 1083, 14220, Prague 4, Czech Republic

^d Department of Physiology, Faculty of Science, Charles University in Prague, Albertov 6, 12843, Prague 2, Czech Republic

^e Loschmidt Laboratories, Department of Experimental Biology and RECETOX, Masaryk University, Kamenice 5/A4, 625 00, Brno, Czech Republic

^f International Centre for Clinical Research, St. Anne's University Hospital, Pekarska 53, 656 91 Brno, Czech Republic

^g National Institute of Mental Health, Topolová 748, 250 67, Klecany, Czech Republic

^h Department of Toxicology and Military Pharmacy, Faculty of Military Health Sciences, University of Defence, Trebesska 1575, 500 01, Hradec Kralove, Czech Republic

ⁱ Department of Pharmaceutical Chemistry and Pharmaceutical Analysis, Faculty of Pharmacy in Hradec Kralove, Charles University, Heyrovského, 1203, Hradec Kralove, Czech Republic

ARTICLE INFO

Article history:

Received 19 February 2021

Received in revised form

29 March 2021

Accepted 31 March 2021

Available online xxx

Keywords:

QSAR

Acetylcholinesterase

Electrophysiology

Glutamate receptor

Ion channel

Pharmacology

in vivo

Tacrine

ABSTRACT

Tacrine is a classic drug whose efficacy against neurodegenerative diseases is still shrouded in mystery. It seems that besides its inhibitory effect on cholinesterases, the clinical benefit is co-determined by NMDAR-antagonizing activity. Our previous data showed that the direct inhibitory effect of tacrine, as well as its 7-methoxy derivative (7-MEOTA), is ensured via a "foot-in-the-door" open-channel blockage, and that interestingly both tacrine and 7-MEOTA are slightly more potent at the GluN1/GluN2A receptors when compared with the GluN1/GluN2B receptors. Here, we report that in a series of 30 novel tacrine derivatives, designed for assessment of structure-activity relationship, blocking efficacy differs among different compounds and receptors using electrophysiology with HEK293 cells expressing the defined types of NMDARs. Selected compounds (**4** and **5**) potently inhibited both GluN1/GluN2A and GluN1/GluN2B receptors; other compounds (**7** and **23**) more effectively inhibited the GluN1/GluN2B receptors; or the GluN1/GluN2A receptors (**21** and **28**). QSAR study revealed statistically significant model for the data obtained for inhibition of GluN1/GluN2B at -60 mV expressed as IC_{50} values, and for relative inhibition of GluN1/GluN2A at $+40$ mV caused by a concentration of $100 \mu M$. The models can be utilized for a ligand-based virtual screening to detect potential candidates for inhibition of GluN1/GluN2A and/or GluN1/GluN2B subtypes. Using *in vivo* experiments in rats we observed that unlike MK-801, the tested novel compounds did not induce hyperlocomotion in open field, and also did not impair prepulse inhibition of startle response, suggesting minimal induction of psychotomimetic side effects. We conclude that tacrine derivatives are promising compounds since they are centrally available subtype-specific inhibitors of the NMDARs without detrimental behavioral side-effects.

© 2021 The Author(s). Published by Elsevier Masson SAS. This is an open access article under the CC BY-NC-ND license (<http://creativecommons.org/licenses/by-nc-nd/4.0/>).

* Corresponding author. Department of Neurochemistry, Institute of Experimental Medicine of the Czech Academy of Sciences, Videnska 1083, 14220, Prague 4, Czech Republic.

** Corresponding author. Biomedical Research Centre, University Hospital Hradec Kralove, Sokolska 581, 50005, Hradec Kralove, Czech Republic.

E-mail addresses: martin.horak@iem.cas.cz (M. Horak), ondrej.soukup@fnhk.cz (O. Soukup).

¹ L.G. and A.M. contributed equally.

1. Introduction

The so-called multitarget-directed ligand (MTDL) paradigm has been widely applied in the last decade to find novel drug candidates against Alzheimer's disease (AD) [1–4]. However, this approach seems to be limited by oversimplified design of novel drug candidates combining pharmacophores with incompatible mechanisms of action, or by reason of irrelevance in the context of disease progression in time [5]. Another limitation is associated with the fact that simple *linking* of the two pharmacophores usually leads to lower drug-likeness, and hence *fused* or *merged* strategies are more preferred [5]. Since AD is currently treated by acetylcholinesterase inhibitors (AChEI) and memantine, an antagonist of *N*-methyl-D-aspartate receptors (NMDAR), a combination of such drugs makes sense, given the fact that impairment of both cholinergic and glutamatergic neurotransmission occurs simultaneously, i.e. in the latter stage of the disease. Hence, Namzaric, a fixed dose combination of donepezil and memantine, was approved by the FDA in 2014 [6].

The dual concept applying inhibition of both AChE and NMDAR based on a *linking* MTDL approach was first pioneered by Simoni et al. who linked galantamine and memantine by a six-membered carbon chain to deliver memagal as a lead structure [7]. It was followed by an *in vivo* study of the shorter-tethered analogue ARN14140, which demonstrated efficacy in preventing cognitive impairment and in its neuroprotective potential [8]. In other research, tacrine-based hybrids with memantine were prepared and evaluated for their *in vitro* affinity towards NMDAR [9,10], and later neuroprotective efficacy was confirmed in the NMDA-induced lesion rat model for the 6-chlorotacrine – memantine hybrid [11]. Notably, the concomitant effect of NMDAR-antagonism and AChE inhibition was established for huperzine-A, a compound approved for AD treatment in China. However, despite high expectations, its dually-acting derivatives [12] together with bis(7)-tacrine [bis(7)-cognitin] [13] have never reached clinical trials.

We have recently summarized that tacrine itself possesses both direct and indirect effects on glutamatergic neurons. Indirect beneficial effect may involve inhibition of Ca^{2+} -activated potassium channels, which prevents membrane repolarization and thus leads to prolonged NMDAR activation and long-term potentiation [14]. Interestingly, the direct effect of tacrine, as well as its 7-methoxy derivative (7-MEOTA), is implemented by inhibition of NMDAR via a “foot-in-the-door” open-channel block, with affinity in the case of 7-MEOTA comparable to that of memantine [15]. We also found that the IC_{50} values for tacrine and 7-MEOTA exhibit the following GluN2 subunit-dependent pattern: $\text{GluN1/GluN2A} < \text{GluN1/GluN2B} < \text{GluN1/GluN2C} = \text{GluN1/GluN2D}$. Interestingly, 7-MEOTA significantly surpassed the neuroprotective effect of both tacrine and memantine in the NMDA-induced lesion rat model, which supports a potential clinical impact [15].

In summary, we hypothesize that the clinical efficacy of tacrine is also co-determined by the NMDAR-antagonizing activity. Thus, compounds structurally related to tacrine can be considered as true MTDLs, and tacrine's structural simplicity ensures its drug-likeness, in contrast to MTDLs created by the *linked* approach. From this standpoint, different tacrine substitutions will deliver various effects on both AChE and NMDAR. In particular, effects on the latter offer a novel approach, and tuning the efficacy and selectivity to different subtypes of NMDARs represents an interesting opportunity in the field of NMDAR antagonists. It is of note that specific inhibitors of GluN1/GluN2B receptors are of interest for their suppression of the negative effects of excitotoxicity [16] and ischemia [17]. Moreover, it has been anticipated that low expression levels of

GluN1/GluN2B receptors in the cerebellum may prevent their side effects [18].

The aim of this study was to develop novel tacrine derivatives with dual effect on cholinesterases and NMDAR, specifically with preference towards GluN1/GluN2A and/or GluN1/GluN2B receptors. Specifically, we synthesized a series of 30 tacrine derivatives and investigated their inhibitory potency towards human recombinant AChE (hAChE) and human plasmatic butyrylcholinesterase (hBChE), and their ability to block GluN1/GluN2A and GluN1/GluN2B receptors at negative and positive membrane potentials. These experiments were followed by analyses of quantitative structure-activity relationships (QSAR) which to the best of our knowledge was performed for the first time ever for tacrine-based compounds. In addition, to follow the potential clinical application of such dually-acting compounds, we have selected the six most promising candidates with more or less balanced activities and characterized them for their ability to cross the blood-brain barrier and for their safety *in vivo*, since a major concern for NMDAR ligands is their psychotomimetic side effects.

2. Design

Tacrine (Fig. 1) was the driving motif in the design of novel compounds (1–30). The critical features in the design of the novel compounds were invested in their basic physicochemical properties as defined by both bioavailability rules (Lipinski rule of 5) [19] and central accessibility (blood-brain barrier score; BBB score) (Table S1) [20]. Physicochemical characteristics are extremely important in drug development, particularly for CNS disorders. Indeed, previous attempts to amalgamate both NMDAR and cholinesterase inhibition properties into one molecule were mostly associated with poor drug-likeness of the final hybrid. 7-MEOTA-adamantylamines [9,10], 6-chlorotacrine-memantine [11], galantamine-memantines [7], benzohomoadamantane-chlorotacrines [21], and amantadine-carbazoles/tetrahydrocarbazoles [22,23], all constructed by the *linking* approach, are a few such examples of developed families possessing dual action against NMDAR and cholinesterases. The translation of their promising *in vitro* properties into *in vivo* conditions was hampered by i) imbalance of their affinities to the relevant targets (NMDAR, hAChE, hBChE); ii) a complicated drug administration protocol not suitable for long-term use in the animal/human (e.g. ARN14140 was injected intracerebroventricularly) [8]; and iii) limited solubility of the drug (e.g. 7-MEOTA-adamantylamine heterodimers) [10]. While the first issue can be addressed by tuning the affinities via structural modifications, the latter two are constrained by their physicochemical properties. Hence, in our study, all the compounds fulfill the criteria to become both CNS and orally available (Table S1). From the chemistry standpoint, we pursued a fundamental structure-activity relationship (SAR) consequent to structural modifications in two regions: i) the substitution by electron-withdrawing and/or electron-donating groups on the aromatic moiety of the basic tacrine scaffold. We have selected distinct positions of derivatization, most of them with the intention to avoid formation of toxic tacrine metabolite, i.e. 7-hydroxytacrine, as reported for hepatotoxic tacrine [24]; and ii) the size of the cycloalkyl moiety attached to the aromatic region, specifically cyclopentane, cyclohexane and cycloheptane rings. There have been numerous studies describing the SAR with respect to hAChE inhibition in tacrine congeners, and a few publications with quantitative evaluation [25–28]. However, the effect of tacrine derivatives on the NMDAR has never been systematically studied.

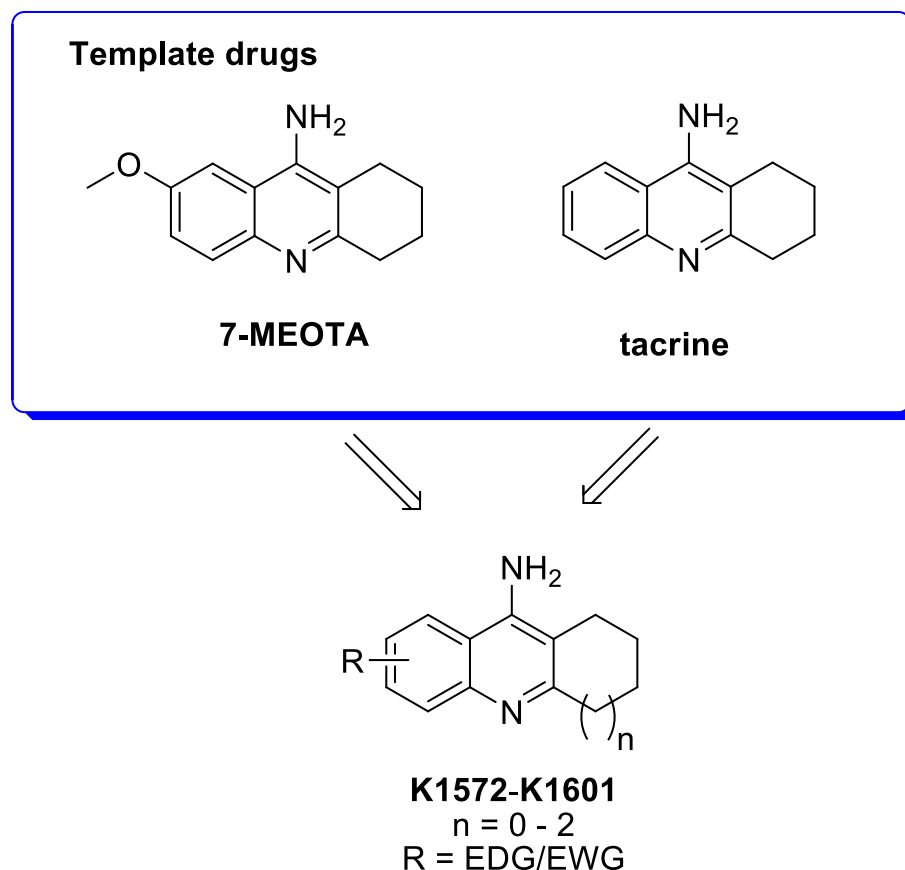


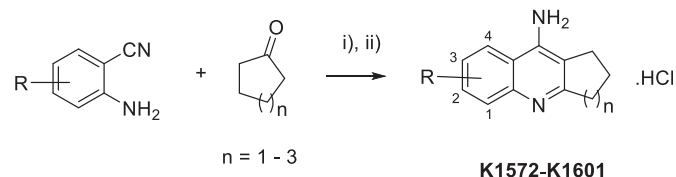
Fig. 1. Design considerations for novel tacrine derivatives **K1572–K1601** possessing dual AChE and NMDAR antagonism properties with tacrine and 7-MEOTA as template drugs.

3. Results and discussion

3.1. Chemistry

A highly efficient one-step procedure was applied for the synthesis of **1–30** (Scheme 1). The crucial aspect in the synthesis was the commercial availability of starting material, namely 2-aminobenzonitrile. The Lewis acid (LA) catalysed Friedländer type condensation for tacrine formation is well established in the literature. The overnight reflux reaction in 1,2-dichloroethane with excellent yields (72%–95%) has been recently described [29]. Another approach, a solvent-free reaction under standard conditions at 130 °C, leads to the desired product with poor to good yields (20%–60%) [25].

In our case, we applied microwave (MW) irradiation to speed up the reaction [30]. Indeed, the full conversion was completed in less than 10 min. Moreover, the solvent-free reaction exhibited mostly excellent yields over 80%. We also found that not all LAs were equally efficient. In some cases, ZnCl_2 led to no reaction at all.



Scheme 1. The reaction of 2-aminobenzonitrile with cyclic ketone leading to the final tacrine derivatives. ZnCl_2 or AlCl_3 were used as LAs in the Friedländer type condensation. Reagents and conditions: i) LA; MW; 10 min; 150 °C; ii) MeOH; HCl (25% in H_2O), RT.

Generally, in the case of the reaction with cyclopentanone, stronger LAs had to be used. In contrast, AlCl_3 always yielded a complete reaction. All the tacrines were converted into their corresponding hydrochloride salts. Compounds were analyzed by a combination of ^1H NMR and ^{13}C NMR spectra, and their identity was confirmed by HRMS. All of them exhibited purity $\geq 97\%$.

3.2. In vitro anti-cholinesterase assay

Modified Ellman's method was applied to assess the inhibitory potency of the novel compounds [31]. The inhibitory potencies of all newly developed compounds are summarized in Table 1. hAChE inhibition is still regarded as crucial in the symptomatic therapy of AD, but it has to be pointed out that hAChE levels decrease with the disease progression, whereas those of hBChE remain stable or become slightly elevated as a compensatory mechanism for the loss of neuronal hAChE activity [32]. For these reasons, we have established the inhibition activity against both hAChE and hBChE. Except for **19**, all the compounds were effective inhibitors of both hAChE and hBChE in a two-digit nanomolar to two-digit micromolar range, with IC_{50} values ranging respectively from 33 nM (**20**) to 22.5 μM (**3**), and from 62 nM (**20**) to 89.9 μM (**15**). With respect to the size of the saturated rings, compounds bearing five- and six-membered rings exhibited slightly increased selectivity towards AChE. Seven-membered congeners showed less profound selectivity; although, hBChE selectivity was rather observed. This accords with the larger hBChE cavity compared to the narrow hAChE gorge, such that larger derivatives should be better accommodated by the hBChE enzyme [33]. 3-Fluoro derivatives (**16–18**) were more potent than 3-chloro derivatives (**7–9**), and those in turn exceeded

Table 1

Inhibitory effect of tacrine derivatives at AChE, BChE and recombinant NMDAR expressed in HEK293 cells.

compound	n	R	GluN1/GluN2A		GluN1/GluN2B		ChE		
			IC ₅₀ ± SEM (μM) (−60 mV)	RI (+40 mV) at 100 μM (%) ^a	IC ₅₀ ± SEM (μM) (−60 mV) ^a	RI (+40 mV) at 100 μM (%)	hAChE IC ₅₀ ± SEM (μM)	hBChE IC ₅₀ ± SEM (μM)	SI (hBChE/ hAChE)
K1572 (1)	1	3-CH ₃	20.46 ± 1.21	30.78 ± 2.03	19.78 ± 2.84	53.74 ± 2.35	10.0 ± 1.0	23.7 ± 2.37	2.37
K1573 (2)	2	3-CH ₃	12.28 ± 1.56	18.54 ± 2.08	13.18 ± 0.91	78.41 ± 2.99	15.5 ± 1.4	13.7 ± 0.4	0.88
K1574 (3)	3	3-CH ₃	27.12 ± 1.97	40.09 ± 2.45	16.58 ± 1.30	50.94 ± 2.69	22.5 ± 1.6	10.6 ± 0.4	0.47
K1575* (4)	1	3-Br	6.31 ± 0.27	75.31 ± 1.85	8.24 ± 0.80	93.22 ± 2.38	5.69 ± 0.28	16.9 ± 1.5	3.03
K1576* (5)	2	3-Br	6.93 ± 1.03	79.33 ± 2.65	8.32 ± 0.97	90.95 ± 3.27	4.79 ± 0.02	20.8 ± 1.2	4.34
K1577 (6)	3	3-Br	13.84 ± 1.25	57.72 ± 4.02	11.81 ± 1.37	91.58 ± 4.02	13.8 ± 0.6	15.1 ± 1.1	1.09
K1578* (7)	1	3-Cl	21.01 ± 0.71	56.49 ± 2.26	8.69 ± 0.60	78.73 ± 4.65	1.58 ± 0.05	6.88 ± 0.65	4.35
K1579 (8)	2	3-Cl	14.79 ± 1.22	47.53 ± 2.31	9.82 ± 1.28	86.54 ± 1.88	1.94 ± 0.07	6.72 ± 0.54	3.46
K1580 (9)	3	3-Cl	20.23 ± 1.74	43.05 ± 2.03	12.00 ± 1.00	88.46 ± 2.94	8.60 ± 0.47	10.3 ± 0.7	1.19
K1581 (10)	1	1,3-diCl	14.63 ± 2.04	33.54 ± 3.58	21.45 ± 1.75	49.11 ± 5.88	13.1 ± 1.0	17.9 ± 0.1	1.36
K1582 (11)	2	1,3-diCl	23.99 ± 1.92	38.24 ± 4.28	37.09 ± 4.77	42.96 ± 6.56	4.34 ± 0.31	14.8 ± 0.4	3.41
K1583 (12)	3	1,3-diCl	20.03 ± 2.03	38.53 ± 5.32	37.86 ± 3.71	43.94 ± 3.78	9.04 ± 0.49	23.8 ± 1.0	2.63
K1584 (13)	1	1,3-diBr	10.24 ± 1.38	55.69 ± 2.27	17.11 ± 1.12	43.34 ± 1.98	15.1 ± 1.0	34% at 100 μM	n/a
K1585 (14)	2	1,3-diBr	15.55 ± 1.62	67.65 ± 5.27	18.70 ± 0.94	40.35 ± 3.24	5.18 ± 0.3	32.0 ± 1.1	6.17
K1586 (15)	3	1,3-diBr	21.52 ± 0.97	80.65 ± 3.16	26.92 ± 5.03	17.32 ± 3.44	15.1 ± 1.4	89.9 ± 7.2	5.95
K1587 (16)	1	3-F	27.96 ± 2.16	28.69 ± 1.15	30.32 ± 1.88	38.40 ± 0.87	0.662 ± 0.02	1.91 ± 0.1	2.88
K1588 (17)	2	3-F	15.44 ± 1.68	41.93 ± 2.09	21.27 ± 1.35	46.77 ± 0.66	0.978 ± 0.051	0.751 ± 0.032	0.77
K1589 (18)	3	3-F	14.47 ± 0.82	38.47 ± 1.61	19.81 ± 1.22	56.01 ± 1.39	0.624 ± 0.025	0.569 ± 0.022	0.911
K1590 (19)	1	4-Cl	27.02 ± 2.94	24.48 ± 2.91	44.88 ± 5.00	23.83 ± 3.22	6% at 100 μM	6% at 100 μM	n/a
K1591 (20)	2	4-Cl	19.61 ± 0.91	34.97 ± 1.40	23.72 ± 1.89	28.96 ± 1.26	0.0334 ± 0.0014	0.062 ± 0.003	1.85
K1592* (21)	3	4-Cl	7.29 ± 0.57	46.73 ± 3.49	22.07 ± 1.11	37.95 ± 5.26	0.223 ± 0.006	0.311 ± 0.016	1.39
K1593 (22)	1	2-CH ₃	7.68 ± 0.79	53.56 ± 1.36	15.59 ± 1.28	62.98 ± 3.07	0.347 ± 0.013	8.44 ± 0.49	24.3
K1594* (23)	2	2-CH ₃	17.05 ± 1.59	51.33 ± 1.44	7.83 ± 0.34	72.00 ± 2.89	0.072 ± 0.003	2.90 ± 0.08	40.2
K1595 (24)	3	2-CH ₃	15.19 ± 1.47	50.05 ± 3.98	9.29 ± 0.54	58.86 ± 5.59	0.104 ± 0.004	1.00 ± 0.03	9.16
K1596 (25)	1	4-CH ₃	21.92 ± 2.18	22.04 ± 2.84	16.55 ± 2.28	37.43 ± 1.76	0.415 ± 0.028	0.471 ± 0.011	1.13
K1597 (26)	2	4-CH ₃	18.48 ± 1.72	40.48 ± 2.16	14.21 ± 0.89	43.06 ± 8.61	0.125 ± 0.007	0.495 ± 0.017	3.96
K1598 (27)	3	4-CH ₃	12.55 ± 1.48	54.29 ± 1.95	17.44 ± 1.43	49.04 ± 6.16	0.255 ± 0.011	0.107 ± 0.006	0.42
K1599* (28)	1	3-OCH ₃	4.16 ± 0.37	66.12 ± 1.88	14.56 ± 1.37	52.05 ± 1.55	8.22 ± 0.35	10.6 ± 0.3	1.23
K1600 (=7-MEOTA) (29)	2	3-OCH ₃	5.05 ± 0.62	77.59 ± 1.52	7.24 ± 0.34	68.84 ± 1.50	10.0 ± 1.0	17.6 ± 0.8	1.76
K1601 (30)	3	3-OCH ₃	20.02 ± 1.29	53.58 ± 2.76	7.67 ± 1.22	69.17 ± 3.59	17.6 ± 0.7	4.41 ± 0.34	0.25
tacrine ^f	—	—	9.1 ± 0.5	Table 2	19.7 ± 1.8	Table 2	0.32 ± 0.013	0.08 ± 0.001	0.25

the activity of 3-bromotacrines (**4–6**). Addition of another halogen into the 1-position decreased the affinity compared to single halogen-substituted analogues, with 1,3-dibromo compounds (**13–15**) being the least active in the whole series. 4-Substituted derivatives revealed inhibition potency increment in the following order: 4-chloro (**20–21**) > 3-chloro (**7–9**) derivatives; however, the 4-chloro substituted compound **19** with a five-membered ring exhibited almost no activity for both ChE. A similar trend in substituent positioning was observed in methyl derivatives, where 2-substitution (**22–24**) was superior to 4-substitution (**25–27**) and 3-substitution (**1–3**), the latter being the least effective towards hAChE. On the other hand, 4-methyl derivatives (**25–27**) were more active than 2-methyl (**22–24**) in the case of hBChE inhibition. The compounds with a 3-methoxy group showed only moderate albeit balanced affinity towards both enzymes. Noteworthy, the study by Recanatini and colleagues highlighted 6-chlorotacrine as the most hAChE active tacrine derivative from the series with single-digit nanomolar IC₅₀ value (IC₅₀ = 9.9 ± 0.3 nM). Other aryl substitutions at the aliphatic six-membered tacrine derivatives ring diminished the activity, except for some amino-substitutions by heptyl or, more preferably, by benzyl appendages [25]. Such observations have also been well documented by us in the family of *N*-alkyl-substituted 7-methoxytacrine derivatives, pointing out that the attachment of

aliphatic alkyl chains improve the hAChE potency [34].

Interestingly, several compounds (**20**, **21**, **23**, **24**, **26**, and **27**) were shown to be more effective in hAChE inhibition than the parent tacrine, although none of the novel compounds surpassed tacrine's hBChE inhibition. Notably, **20** was the most potent ChE inhibitor tested (hAChE IC₅₀ = 0.033 ± 0.001 μM; BChE IC₅₀ = 0.062 ± 0.003 μM).

3.3. Interaction with NMDAR

Next, we aimed to examine the inhibitory effect of the new derivatives at the most common types of NMDARs in the adult human forebrain, GluN1/GluN2A and GluN1/GluN2B [35], as expressed in HEK293 cells. As we needed to screen a large set of novel derivatives with these two NMDAR types, we initially examined each compound using three different concentrations (1, 10, 100 μM) at two membrane potentials (−60 mV, +40 mV, Table 1); we did not examine concentrations >100 μM, due to physiological irrelevance and due to the fact that some compounds exhibited limited solubility when dissolved in the extracellular recording solution (ECS). Consistently with our previous data [15], we observed that at membrane potential −60 mV, 7-MEOTA is slightly more potent at the GluN1/GluN2A receptors when compared to the GluN1/GluN2B receptors (IC₅₀ values: ~5 versus

~7 μM). Interestingly, the novel compounds exhibited IC_{50} values ranging from ~4 μM to ~45 μM at both the GluN1/GluN2A receptors and GluN1/GluN2B receptors, and we observed that in most cases there is no preference for the GluN1/GluN2A receptors over the GluN1/GluN2B receptors (Table 1). Notably, the reference drug memantine showed the IC_{50} value of 1.34 ± 0.08 and 0.78 ± 0.09 on GluN1/GluN2A and GluN1/GluN2B respectively [36]. With respect to our measurements at membrane potential 40 mV, we indeed observed, consistently with our previous data [15], that tacrine and its derivatives exhibited reduced inhibitory effect at both NMDAR types (Table 1). Due to the lower inhibitory activity and the screening nature of our investigation at this stage (only three concentrations were tested), we expressed the inhibitory effect of each compound at this membrane potential as the relative inhibition (RI (40 mV)). Similarly to our conclusion at negative membrane potential, RI (40 mV) values exhibited no clear preference for the GluN1/GluN2A receptors over the GluN1/GluN2B (Table 1). Nevertheless, to investigate the structure-activity relationship of tacrine derivatives on both types of NMDAR we performed QSAR analysis. Moreover, based on the results obtained from ChE/NMDA evaluation we selected 6 compounds (**4**, **5**, **7**, **21**, **23** and **28**) with the most interesting properties for detailed evaluation of NMDAR properties and for *in vivo* tests. Specifically, we selected **4** and **5** for their relatively similar affinity towards all studied targets and **7** for its approximately 10-fold higher affinity toward ChE over the GluN1/GluN2B subtype. Furthermore, we chose **21** as a non-selective sub-micromolar ChE inhibitor, **23** as selective AChE inhibitor with the preference of GluN1/GluN2B subtype and **28** as a compound with the preference of GluN1/GluN2A subtype.

The experimental data obtained from the electrophysiological measurements with three concentrations of each compound (1, 10, 100 μM) were fitted by Equation (2) (see the methods section); the resulting values of IC_{50} , Hill coefficient (h), and numbers of analyzed cells (n) recorded at membrane potential of -60 mV were obtained. IC_{50} (in μM) values and relative inhibition values (RI (+40 mV)) calculated for the measurements at membrane potential +40 mV are shown. Data are shown as mean \pm SEM (standard error of the mean). Experimental details (h coefficient and n) are listed in Table S2. *Compounds selected for detailed assessment where $\text{IC}_{50} \pm \text{SEM}$ value was established in addition to RI at 100 μM (Table 2). ¹ The data obtained from Ref. [15].

3.4. Quantitative structure-activity relationships (QSAR)

Next, analyses of Quantitative Structure-Activity Relationships were carried out to understand how the biological effects depend on the structural properties of the studied molecules. Concerning the inhibitory potency towards the GluN1/Glu2A unit, the Partial Least Squares (PLS) analysis provided a statistically significant model correlating molecular descriptors and experimentally determined observables in the relative inhibition of these receptors

evoked by 100 μM of the tested compound at +40 mV (2A-RI-40). The model uses four principal components and shows statistically significant coefficient of determination $R^2 = 0.89$ and cross-validated coefficient of determination $Q^2 = 0.79$ (Fig. S1). The 45 most significant variables contributing to explanation of experimental values are shown in the Variable Importance to Projections (VIP) plot (Fig. S2). Validation of the QSAR model for 2A-RI-40 activities by cross-validation and permutation testing is illustrated in SI (Fig. S3). This exhaustive test proved that the QSAR model loses its predictivity when the input data are randomly permuted.

The most influential molecular descriptors in this QSAR model, namely Mor15 m, GeomPetitj, GoemShape1, BCUTs-11, and MATS1p, belong among 3D or 2D topological indices weighted by certain distance, electronegativity or intrinsic state. Apart from these complex molecular descriptors, significant influence on the biological activity was exhibited also by lipophilicity (SlogP_VSA6), suggesting that more lipophilic compounds elicit stronger biological response, i.e., higher inhibitory potency towards the GluN1/Glu2A subunit.

Furthermore, PLS analysis provided also a statistically significant model correlating molecular descriptors and experimentally determined inhibitory potency on the GluN1/Glu2B unit at -60mV, expressed as the IC_{50} values (2B- IC_{50}). The model uses four principal components and shows a significant coefficient of determination $R^2 = 0.89$ and cross-validated coefficient of determination $Q^2 = 0.73$ (Fig. S4). The 54 most significant variables contributing to explanation of experimental values are shown in the VIP plot (Fig. S5). The validation test of the QSAR model proving its high sensitivity to data mismatch is described in Fig. S6. According to the VIP values, the most influential molecular descriptors in this QSAR model are represented by BalabanJ, Xc-5d, MATS4pe, MDEC-33, and Xpc-5d, which are 2D/3D topological indices weighted by certain geometrical or electronic parameters. It was discovered in the plot of loadings for the two most significant principal components in the QSAR model that the molecular descriptors form several features and groups, suggesting intercorrelations among the descriptors.

However, the proposed QSAR models are applicable at the above-mentioned statistical level of significance only if all involved molecular descriptors are taken into consideration. Due to the high complexity of PLS based models, this QSAR can be utilized especially in a ligand-based virtual screening to select potential candidates for inhibition of GluN1/Glu2A and/or GluN1/Glu2B rather than for intuitive design of novel chemical structures with significant activity for the receptor. Further details on the selected descriptors may be found online (<https://mordred-descriptor.github.io/documentation/master/descriptors.html>).

In summary, both GluN1/GluN2A and GluN1/GluN2B receptors have a highly homologous amino acid composition in the ion channel region [35], which likely contains a binding site for the studied inhibitors [15]. Therefore, the significance of similar

Table 2

Dose-response relationships for inhibition of the selected tacrine derivatives at GluN1/GluN2A and GluN1/GluN2B receptors.

code name	GluN1/GluN2A		GluN1/GluN2B	
	$\text{IC}_{50} \pm \text{SEM}$ (-60 mV)	$\text{IC}_{50} \pm \text{SEM}$ (+40 mV)	$\text{IC}_{50} \pm \text{SEM}$ (-60 mV)	$\text{IC}_{50} \pm \text{SEM}$ (+40 mV)
29	4.70 \pm 0.30	49.31 \pm 1.97	7.24 \pm 0.34	51.02 \pm 2.99
4	6.12 \pm 0.12	51.35 \pm 1.77	6.98 \pm 0.39	23.00 \pm 1.27
5	6.58 \pm 0.76	45.89 \pm 3.23	7.80 \pm 0.48	12.75 \pm 1.36
7	22.56 \pm 0.83	84.16 \pm 5.75	9.39 \pm 0.47	27.66 \pm 1.11
23	21.55 \pm 1.38	98.56 \pm 5.06	8.03 \pm 0.52	41.82 \pm 2.74
21	7.66 \pm 0.35	111.60 \pm 5.32	26.14 \pm 0.93	146.40 \pm 10.86
28	5.16 \pm 0.58	66.80 \pm 4.30	16.06 \pm 1.15	88.89 \pm 4.66
tacrine ¹	9.1 \pm 0.5	84.6 \pm 1.6	19.7 \pm 1.8	168.8 \pm 9.3

molecular descriptors was expected when analyzing structure-activity relationships. Both models employ analogous descriptors (complex topological indexes) for the explanation of the biological activity. This is in accordance with the expected binding of studied molecules to the molecular pore, which will primarily depend on the size and conformational flexibility of studied inhibitors. The model constructed for the determined activities 2A-RI-40 additionally employs also the descriptor of lipophilicity (SlogP_VSA6). This descriptor's statistical importance suggests that hydrophobic interactions are the additional driving force for the binding of studied compounds to the receptor, besides the size and shape of the molecules captured by various topological complexes. In addition, different functional and pharmacological properties of GluN1/GluN2A and GluN1/GluN2B receptors, such as desensitization or open probability, may co-determine different sensitivity towards inhibitors [38]. Overall, the two models are highly similar in their composition as well as in their predictive power. Therefore, the individual models are specifically helpful for predictive purposes.

3.5. Detailed electrophysiological analysis of selected tacrine compounds at both GluN1/GluN2A and GluN1/GluN2B receptors

To pursue the pre-clinical aspect of our study, we selected the 6 most promising compounds which notwithstanding interaction with ChE: potently inhibited both GluN1/GluN2A and GluN1/GluN2B receptors (**4** and **5**); more potently inhibited the GluN1/GluN2B receptors (**7** and **23**); more potently inhibited the GluN1/GluN2A receptors (**21** and **28**) (see Table 1). Firstly, we used the same electrophysiological experimental approach as above, but with five different concentrations of tacrine derivatives (1, 3, 10, 30, 100 μ M); we then obtained the respective IC_{50} values for each compound at two membrane potentials (-60 mV, $+40$ mV) at both NMDAR types (Table 2, Fig. 2) which corresponds well to the data shown in Table 1.

The electrophysiological data obtained using five concentrations of each compound (1, 3, 10, 30, 100 μ M) from HEK293 cells expressing the indicated NMDARs were fitted by Equation (1); the resulting values of IC_{50} (in μ M) recorded at membrane potentials of -60 mV or $+40$ mV are shown as the mean \pm SEM (standard error of the mean). Experimental details (Hill's coefficient (h) and number of analyzed cell (n) are listed in Table S3).¹ The data obtained from Ref. [15].

3.6. Blood-brain barrier permeability

In compliance with RRR strategy for using laboratory animals, the blood-brain barrier permeability (BBB) was evaluated for six selected candidates first *in vitro* via the MDCK cell-based assay [39,40], and subsequently verified *in vivo* on a small number of mice. The cell-based assay predicted high BBB permeability, similar to that obtained for tacrine or donepezil (Table S4). *In vivo* pharmacokinetic experiments were performed on mice by injecting i.p. 5 mg kg⁻¹ of the six selected candidates, and their concentration levels measured in the plasma and brain tissue by HPLC-MS at two time points, after 15 min and 60 min (a group of 3 animals per each time point). The plasma and brain distribution of the tested compounds at the two time intervals are shown in Table 3. It is obvious that all compounds are able to reach the brain, as in the case of the parent tacrine; however, in contrast they are relatively quickly excreted [41]. In the 15th minute the brain/plasma ratios were found to vary from 33% in the case of **21**–138% in the case of **28**. The brain/plasma ratio data suggests that **5** and **28** tend to accumulate in the brain [41,42], whereas compound **21** may be subject to some efflux mechanism. Such result confirms that although all the

compounds are available in the CNS, levels at the 60th min interval in both plasma and brain suggest quick elimination from the organism.

3.7. Behavioral assessment of side effects

Besides their beneficial effects, NMDAR antagonists as well as AChEIs may possess side effects. Specifically, the use of numerous antagonists of NMDAR is limited by psychotomimetic effects [43–45], manifested in rodents as a behavioral syndrome including hyperlocomotion and deficits of sensorimotor gating [46–48]. On the other hand, behavioral side effects of AChEIs may involve suppression of locomotor activity [49,50]. Therefore, we assessed the acute effect of the six selected substances (**4**, **5**, **7**, **21**, **23** and **28**; 1 and 5 mg/kg, administered i.p. 15 min prior to the experiment) on spontaneous locomotor activity in open field, and prepulse inhibition of acoustic startle response in rats in order to investigate the risk of the aforementioned side effects. For comparison, the effects of 7-MEOTA (5 mg/kg) and the NMDAR non-competitive antagonist MK-801 are shown as well.

Analysis of distance moved in open field (1 mg/kg doses) revealed significant effect of treatment (ANOVA; $F(6, 37) = 6.269$, $P = 0.0001$). Compound **21** decreased locomotor activity ($P < 0.0001$ vs. DMSO; Bonferroni post hoc test; Fig. 3A). At a dose of 5 mg/kg, a significant effect of treatment was observed, too (Brown-Forsythe ANOVA; $F^*(8, 13.37) = 38.00$, $P < 0.0001$). Dunnett's T3 multiple comparisons test showed that the distance moved by the animals from groups **4**, **5**, **7**, **21**, **23** (5 mg/kg for all) was significantly lower than that of the control DMSO group ($P = 0.0194$, $P = 0.0374$, $P = 0.0001$, $P < 0.0001$ and $P = 0.0013$, respectively), while MK-801 (0.2 mg/kg), as expected, significantly increased the locomotion ($P = 0.0098$; Fig. 3B).

Next, we investigated the effect of the tested compounds on prepulse inhibition of acoustic startle response (% PPI). At a dose of 1 mg/kg, the compounds did not affect PPI (Fig. 3C). ANOVA of PPI for the compounds at a 5 mg/kg dose showed a significant effect of treatment ($F(8, 48) = 7.377$, $P < 0.0001$), with Bonferroni post hoc test revealing the expected deleterious effect of MK-801 (0.3 mg/kg, $P < 0.0001$ vs. DMSO; Fig. 3D). The results thus indicated that unlike MK-801, all the tested compounds at both doses were free of hyperlocomotion-inducing effects in open field, and they did not impair prepulse inhibition of startle response, suggesting low risk of induction of psychotomimetic side effects. This fact is of great importance, given that serious psychotomimetic effects represent a major limitation for the use of many NMDAR antagonists [45].

On the other hand, substances **4**, **5**, **7**, **21** and **23**, when administered at the higher dose, considerably suppressed locomotor activity in the open field. As AChEIs may suppress locomotor activity [49,50], we suggest that the observed effect may be at least partially exerted via inhibition of hAChE. It seems to be corroborated by the fact that **28** and 7-MEOTA, the only compounds which at a dose of 5 mg/kg did not decrease the locomotor activity, represent the least potent AChEIs of all the tested compounds. By contrast, hypo-locomotion was most prominent in animals treated with **21** (5 mg/kg), a potent inhibitor of both AChE and BChE. Moreover, compound **21**, unlike the other compounds, decreased locomotion even at the lower tested dose (1 mg/kg). However, the *in vivo* mechanisms of action seem to be complex, and simultaneous involvement of other mechanisms in the hypolocomotion-inducing effect cannot be excluded, as the extent of suppression of locomotion does not appear to correspond exactly to the IC_{50} for hAChE. Compound **23**, the most potent inhibitor of hAChE, did not induce the most prominent locomotion-decreasing effect. Notably, **21** exerts about 10-fold more potent inhibition of BChE than **23**, perhaps explaining the more pronounced behavioral effect of **21** and suggesting that

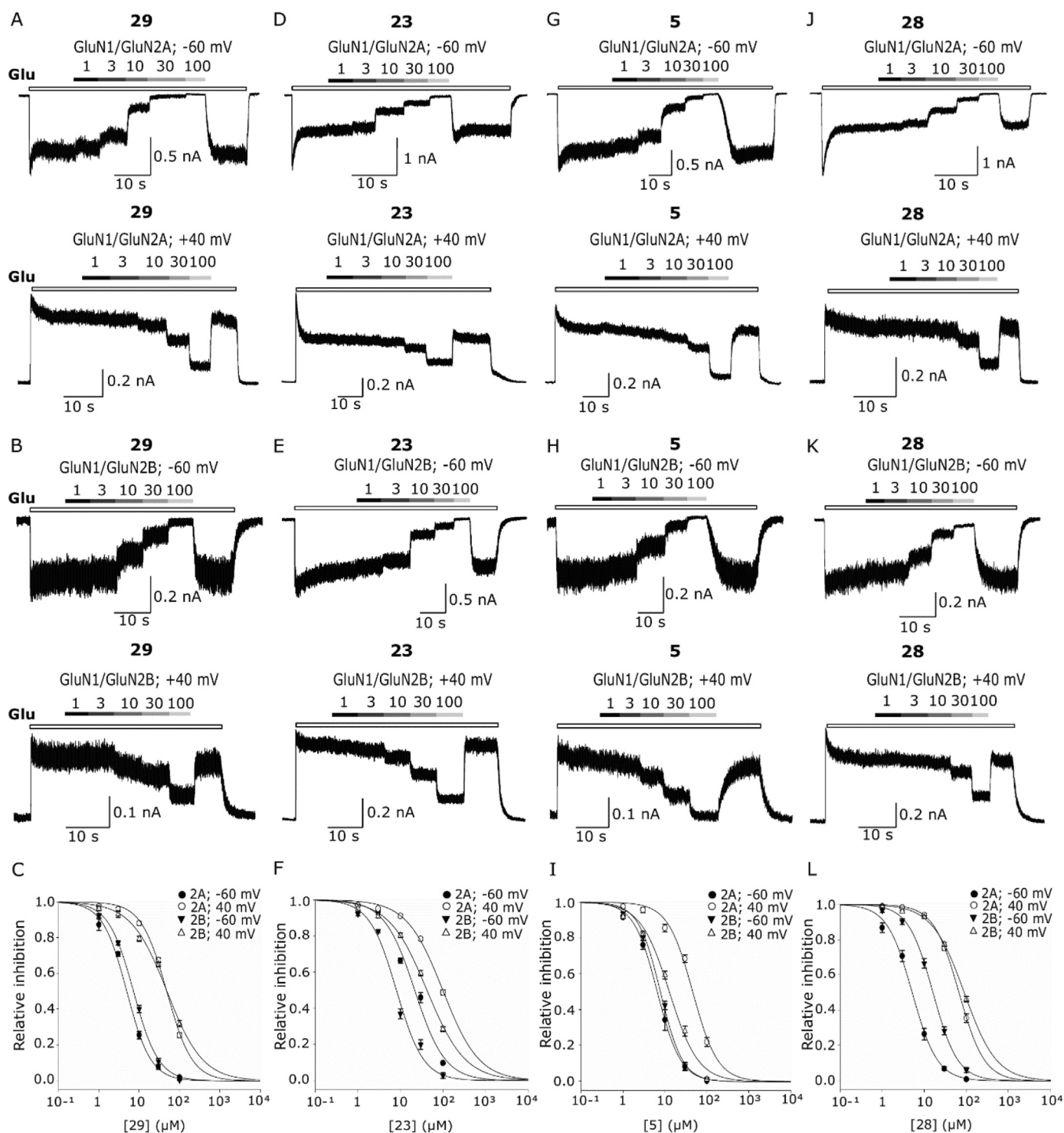


Fig. 2. The selected most potent derivatives of tacrine. Representative responses of tacrine's derivatives at membrane potentials of -60 mV and $+40$ mV from HEK293 cells transfected with GluN1/GluN2A (A,D,G,J) and GluN1/GluN2B (B,E,H,K) receptors; the identities of the derivatives are shown above each current trace with a concentration scale (1–100 μ M) with co-application of 1 mM glutamate (Glu). Concentration-inhibition curves for **29** (C), **23** (F), **5** (I), **28** (L) were obtained by fitting the experimental data from GluN1/GluN2A and GluN1/GluN2B receptors at -60 and $+40$ mV with Equation (1).

inhibition of BChE or the ratio of hBChE/hAChE inhibition might also play a role in the suppression of locomotor activity. These findings seem to be in accordance with these of Pan et al. [51], who compared the effect of tacrine and bis(7)-tacrine on locomotor activity, revealing that tacrine, despite its much less potent inhibition of AChE, decreased the locomotion more profoundly.

Interestingly, tacrine and bis(7)-tacrine show different hBChE/hAChE IC_{50} ratios (0.41 and 99.38 respectively) [52], possibly explaining the locomotion-decreasing potential of tacrine and perhaps mirroring our situation with **21** and **23**. Correspondingly [4], suggest that higher selectivity towards hAChE may be associated with lower risk of certain side effects [53].

Table 3

In vivo availability of selected compounds in the plasma and brain (mice, dose 5 mg/kg, i.p.).

Compound	Concentration (nM) 15th min		Concentration (nM) 60th min		Brain/plasma ratio (%; 15th min)
	Plasma	Brain	Plasma	Brain	
4	2522	1176	154	116	47
5	1334	1376	170	218	103
7	1657	1003	389	173	61
21	2297	762	185	32	33
23	1304	731	87	251	56
29	1673	2315	207	326	138

In summary, the selected compounds were found to be free of psychotomimetic effects of NMDAR antagonists. The only observed side effect, manifested as suppression of locomotor activity and presented at the higher of the tested doses, may represent an expected side effect associated with the drugs' mechanism of action, and hopefully should not appreciably limit the potential use of the tested substances. These favorable findings justify future testing of their therapeutic *in vivo* effects.

4. Conclusions

In this work we have prepared a series of 30 novel tacrine derivatives designed for assessment of structure-activity relationships on the NMDARs. We have shown that, apart of the inhibitory activity towards cholinesterases, selected compounds (**4** and **5**) potentially non-selectively inhibit both GluN1/GluN2A and GluN1/GluN2B receptors; compounds (**7** and **23**) more potently inhibited the GluN1/GluN2B receptors; compounds (**21** and **28**) more

potently inhibited GluN1/GluN2A receptors. The QSAR analysis revealed significant correlation for data obtained for inhibition of GluN1/Glu2B at -60mV and for relative inhibition of GluN1/Glu2A at $+40\text{mV}$ respectively, which can be used in ligand-based virtual screening to detect potential NMDAR ligands. The most influential molecular descriptors were found the 3D or 2D weighted topological indices namely Mor15 m, GeomPetitj, GoemShapel, BCUTs-11, and MATS1p for the GluN1/Glu2A subunit and BalabanJ, Xc-5d, MATS4pe, MDEC-33, and Xpc-5d for the GluN1/Glu2B subunit. Apart from that, lipophilicity showed significant influence on the biological activity.

From the (pre-)clinical point of view, we observed in rats that the tested novel compounds did not induce hyperlocomotion, neither impaired the prepulse inhibition of startle response. Thus despite of proved CNS availability of this class of compounds absence of side-effects typical for blockers of NMDA receptors was observed. Thus, the data have indicated that tacrine derivatives are promising dual-acting compounds, which in addition to their anti-ChE effects, act as centrally available subtype-specific inhibitors of the NMDARs without negative behavioral side effects.

5. Experimental section

5.1. General synthetic methods

Column chromatography was performed using silica gel 100 at atmospheric pressure (70–230-mesh ASTM, Fluka, Prague, Czech Republic). Analytical thin-layer chromatography was carried out using plates coated with silica gel 60 with the fluorescent indicator F254 (Merck, Prague, Czech Republic). The thin-layer chromatography plates were visualized by exposure to ultraviolet light

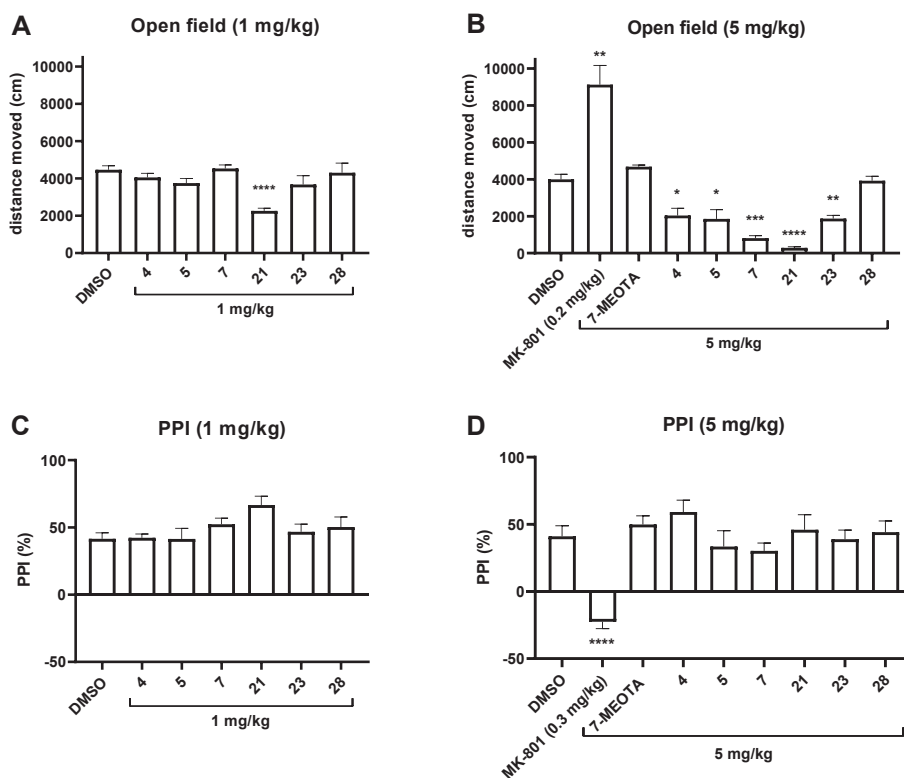


Fig. 3. Behavioral effects of compounds **4**, **5**, **7**, **21**, **23** and **28**. Graphs show distance moved in open field by rats treated with the tested compounds at doses of 1 mg/kg (A) and 5 mg/kg (B), and prepulse inhibition of acoustic startle response in rats treated with the compounds at doses of 1 mg/kg (C) and 5 mg/kg (D). * $P < 0.05$, ** $P < 0.01$, *** $P < 0.001$ and **** $P < 0.0001$ compared to DMSO.

(254 nm) or using the detection reagents phosphomolybdic acid (PMA) and *p*-anisaldehyde (PERNOD). All the NMR spectra were recorded on a Varian S500 spectrometer (500 MHz for ^1H and 126 MHz for ^{13}C). Chemical shifts are reported in δ ppm referenced to residual solvent signals (for ^1H NMR and ^{13}C NMR: chloroform-*d* (CDCl_3 ; 7.26 (D) or 77.16 (C) ppm), methanol-*d*₄ (CD_3OD ; 3.35, 4.78 (D), or 49.3 (C) ppm), or dimethylsulfoxide-*d*₆ ($\text{DMSO-}d_6$; 2.50 (D) or 39.7 (C) ppm). The chemicals were purchased from Sigma-Aldrich Co., LLC (Prague, Czech Republic) and were used without additional purification. A CEM Explorer SP 12 S was used for the MW-assisted reactions. The final compounds were analyzed by high performance liquid chromatography (HPLC) with mass spectrometric detection (MS) using a Dionex Ultimate 3000 RS UHPLC system coupled with a Q Exactive Plus Orbitrap mass spectrometer (Thermo Fisher Scientific, Bremen, Germany) to obtain high-resolution mass spectra (HRMS). Gradient LC analysis confirmed >97% purity.

5.2. Synthesis

5.2.1. General procedure for tacrine derivatives formation

The appropriately-substituted starting 2-amino-benzonitrile (1.0 eq); lewis acid (LA; 2.0 eq); and cyclopentanone, cyclohexanone, or cycloheptanone (2 mL) were challenged by MW irradiation for 10 min at 150 °C. The resulting solid was diluted with 2 M NaOH (3 mL) and dichloromethane (DCM) 2 mL and stirred for 30 min. The solution was diluted by another 2 M NaOH (20 mL) and washed three times with DCM (3 × 20 mL). The organic layers were collected, dried with anhydrous Na_2SO_4 , and filtered, and the filtrate concentrated. The residue was purified by column chromatography to give the crude product as a base. The base was dissolved in MeOH (10 mL) and HCl (25% in H_2O ; 1.5 mL) and stirred overnight. The solution was concentrated and dried to give crude hydrochloride product.

7-methyl-1*H*,2*H*,3*H*-cyclopenta[*b*]quinolin-9-amine hydrochloride (1): 2-amino-5-methylbenzonitrile (180 mg; 1.36 mmol); AlCl_3 (363 mg; 2.72 mmol). Purified by column chromatography using mobile phase DCM/MeOH/ NH_4OH (7:1:0.1) to give the product as a brownish solid. Yield 83%; mp at 252 °C with decomposition.

^1H NMR (500 MHz, $\text{DMSO-}d_6$) δ 8.04 (s, 1H), 7.64 (d, $J = 8.5$ Hz, 1H), 7.47–7.39 (m, 1H), 7.06 (bs, 2H), 2.96 (t, $J = 7.7$ Hz, 2H), 2.81 (t, $J = 7.3$ Hz, 2H), 2.44 (s, 3H), 2.08 (p, $J = 7.6$ Hz, 2H). ^{13}C NMR (126 MHz, $\text{DMSO-}d_6$) δ 163.06, 148.31, 143.37, 132.99, 131.37, 125.08, 121.73, 116.91, 113.89, 33.55, 27.82, 22.30, 21.29. HRMS (HESI⁺): $[\text{M}+\text{H}]^+$: calculated for $\text{C}_{13}\text{H}_{15}\text{N}_2^+$ (m/z): 199.1230; found: 199.1229. HPLC purity >99%.

7-methyl-1,2,3,4-tetrahydroacridin-9-amine hydrochloride (2): 2-amino-5-methylbenzonitrile (315 mg; 2.38 mmol); ZnCl_2 (648 mg; 4.76 mmol). Purified by column chromatography using mobile phase DCM/MeOH/ NH_4OH (9:1:0.1) to give the product as a brownish solid. Yield 98%; mp 154 °C.

^1H NMR (500 MHz, CD_3OD) δ 7.81 (dd, $J = 1.9, 1.0$ Hz, 1H), 7.59 (d, $J = 8.6$ Hz, 1H), 7.40 (dd, $J = 8.6, 1.8$ Hz, 1H), 2.88 (t, $J = 6.1$ Hz, 2H), 2.58 (t, $J = 6.2$ Hz, 2H), 2.48 (s, 3H), 1.97–1.83 (m, 4H). ^{13}C NMR (126 MHz, CD_3OD) δ 156.99, 151.01, 144.28, 134.76, 132.35, 126.31, 121.47, 117.96, 110.54, 33.31, 24.51, 23.75, 23.63, 21.60. HRMS (HESI⁺): $[\text{M}+\text{H}]^+$: calculated for $\text{C}_{14}\text{H}_{17}\text{N}_2^+$ (m/z): 213.1386; found: 213.1383. HPLC purity >99%.

2-methyl-6*H*,7*H*,8*H*,9*H*,10*H*-cyclohepta[*b*]quinolin-11-amine hydrochloride (3): 2-amino-5-methylbenzonitrile (180 mg; 1.36 mmol); AlCl_3 (363 mg; 2.72 mmol). Purified by column chromatography using mobile phase DCM/MeOH/ NH_4OH (7:1:0.1) to give the product as a brownish solid. Yield 81%; mp 103 °C.

^1H NMR (500 MHz, $\text{DMSO-}d_6$) δ 7.99 (d, $J = 1.7$ Hz, 1H), 7.61 (d,

$J = 8.5$ Hz, 1H), 7.40 (dd, $J = 8.5, 1.8$ Hz, 1H), 6.71 (bs, 2H), 3.04–2.95 (m, 2H), 2.83–2.76 (m, 2H), 2.44 (s, 3H), 1.79 (p, $J = 6.3$ Hz, 2H), 1.63 (p, $J = 5.4$ Hz, 2H), 1.55 (p, $J = 5.6$ Hz, 2H). ^{13}C NMR (126 MHz, $\text{DMSO-}d_6$) δ 161.79, 148.32, 142.30, 133.12, 130.90, 126.02, 121.68, 117.36, 114.29, 37.74, 31.64, 27.57, 26.56, 25.30, 21.41. HRMS (HESI⁺): $[\text{M}+\text{H}]^+$: calculated for $\text{C}_{15}\text{H}_{19}\text{N}_2^+$ (m/z): 227.1543; found: 227.154. HPLC purity >99%.

7-bromo-1*H*,2*H*,3*H*-cyclopenta[*b*]quinolin-9-amine hydrochloride (4): 2-amino-5-bromobenzonitrile (154 mg; 0.782 mmol); ZnCl_2 (213 mg; 1.563 mmol). Purified by column chromatography using mobile phase DCM/MeOH/ NH_4OH (15:1:0.1) to give the product as an orange solid. Yield 77%; mp at 247 °C with decomposition.

^1H NMR (500 MHz, $\text{DMSO-}d_6$) δ 8.39 (d, $J = 1.9$ Hz, 1H), 7.65–7.54 (m, 2H), 6.53 (bs, 2H), 2.87 (t, $J = 7.7$ Hz, 2H), 2.80 (t, $J = 7.3$ Hz, 2H), 2.14–1.95 (m, 2H). ^{13}C NMR (126 MHz, $\text{DMSO-}d_6$) δ 167.45, 147.45, 145.58, 130.77, 130.67, 124.58, 119.17, 115.48, 114.34, 34.71, 27.82, 22.31. HRMS (HESI⁺): $[\text{M}+\text{H}]^+$: calculated for $\text{C}_{12}\text{H}_{12}\text{BrN}_2^+$ (m/z): 263.0178; found: 263.0176. HPLC purity >99%.

7-bromo-1,2,3,4-tetrahydroacridin-9-amine hydrochloride (5): 2-amino-5-bromobenzonitrile (156 mg; 0.792 mmol); ZnCl_2 (216 mg; 1.58 mmol). Purified by column chromatography using mobile phase DCM/MeOH/ NH_4OH (9:1:0.1) to give the product as a light orange solid. Yield 72%; mp at 274 °C with decomposition.

^1H NMR (500 MHz, $\text{DMSO-}d_6$) δ 8.42 (d, $J = 1.8$ Hz, 1H), 7.60–7.51 (m, 2H), 6.44 (bs, 2H), 2.80 (t, $J = 6.0$ Hz, 2H), 2.53 (t, $J = 6.1$ Hz, 2H), 1.86–1.74 (m, 4H). ^{13}C NMR (126 MHz, $\text{DMSO-}d_6$) δ 158.29, 147.61, 145.18, 130.98, 130.42, 124.43, 118.54, 115.44, 109.96, 33.71, 23.84, 22.67, 22.56. HRMS (HESI⁺): $[\text{M}+\text{H}]^+$: calculated for $\text{C}_{13}\text{H}_{14}\text{BrN}_2^+$ (m/z): 277.0335; found: 277.0333. HPLC purity >99%.

2-bromo-6*H*,7*H*,8*H*,9*H*,10*H*-cyclohepta[*b*]quinolin-11-amine hydrochloride (6): 2-amino-5-bromobenzonitrile (155 mg; 0.787 mmol); ZnCl_2 (214 mg; 1.57 mmol). Purified by column chromatography using mobile phase DCM/MeOH/ NH_4OH (9:1:0.1) to give the product as an orange solid. Yield 88%; mp at 231 °C with decomposition.

^1H NMR (500 MHz, $\text{DMSO-}d_6$) δ 8.44–8.32 (m, 1H), 7.57 (d, $J = 2.0$ Hz, 2H), 6.42 (bs, 2H), 2.99–2.89 (m, 2H), 2.81–2.74 (m, 2H), 1.78 (p, $J = 5.9$ Hz, 2H), 1.61 (p, $J = 5.5$ Hz, 2H), 1.54 (p, $J = 5.6$ Hz, 2H). ^{13}C NMR (126 MHz, $\text{DMSO-}d_6$) δ 164.92, 146.38, 145.06, 130.82, 130.71, 124.78, 119.45, 116.03, 115.11, 31.73, 27.75, 26.71, 25.48. HRMS (HESI⁺): $[\text{M}+\text{H}]^+$: calculated for $\text{C}_{14}\text{H}_{16}\text{BrN}_2^+$ (m/z): 291.0491; found: 291.0488. HPLC purity >99%.

7-chloro-1*H*,2*H*,3*H*-cyclopenta[*b*]quinolin-9-amine hydrochloride (7): 2-amino-5-chlorobenzonitrile (173 mg; 1.134 mmol); AlCl_3 (302 mg; 2.27 mmol). Purified by column chromatography using mobile phase DCM/MeOH/ NH_4OH (9:1:0.1) to give the product as a brownish solid. Yield 82%; mp at 266 °C with decomposition.

^1H NMR (500 MHz, $\text{DMSO-}d_6$) δ 8.25 (d, $J = 2.4$ Hz, 1H), 7.67 (d, $J = 8.9$ Hz, 1H), 7.47 (dd, $J = 8.9, 2.3$ Hz, 1H), 6.52 (bs, 2H), 2.88 (t, $J = 7.7$ Hz, 2H), 2.80 (t, $J = 7.3$ Hz, 2H), 2.10–1.97 (m, 2H). ^{13}C NMR (126 MHz, $\text{DMSO-}d_6$) δ 167.38, 147.27, 145.67, 130.47, 128.19, 127.18, 121.41, 118.55, 114.34, 34.68, 27.81, 22.33. HRMS (HESI⁺): $[\text{M}+\text{H}]^+$: calculated for $\text{C}_{12}\text{H}_{12}\text{ClN}_2^+$ (m/z): 219.0684; found: 219.0681. HPLC purity >99%.

7-chloro-1,2,3,4-tetrahydroacridin-9-amine hydrochloride (8): 2-amino-5-chlorobenzonitrile (177 mg; 1.16 mmol); AlCl_3 (309 mg; 2.32 mmol). Purified by column chromatography using mobile phase DCM/MeOH/ NH_4OH (9:1:0.1) to give the product as a brownish solid. Yield 66%; mp at 247 °C with decomposition.

^1H NMR (500 MHz, $\text{DMSO-}d_6$) δ 8.28 (d, $J = 2.3$ Hz, 1H), 7.62 (d, $J = 8.9$ Hz, 1H), 7.46 (dd, $J = 9.0, 2.3$ Hz, 1H), 6.42 (bs, 2H), 2.80 (t, $J = 6.0$ Hz, 2H), 2.53 (t, $J = 6.1$ Hz, 2H), 1.91–1.69 (m, 4H). ^{13}C NMR (126 MHz, $\text{DMSO-}d_6$) δ 158.22, 147.66, 145.07, 130.30, 128.40, 127.11,

121.22, 117.92, 109.94, 33.73, 23.85, 22.70, 22.58. HRMS (HESI⁺): [M+H]⁺: calculated for C₁₃H₁₄ClN₂⁺ (*m/z*): 233.0840; found: 233.0837. HPLC purity >99%.

2-chloro-6H,7H,8H,9H,10H-cyclohepta[b]quinolin-11-amine hydrochloride (9): 2-amino-5-chlorobenzonitrile (181 mg; 1.186 mmol); AlCl₃ (316 mg; 1.372 mmol). Purified by column chromatography using mobile phase DCM/MeOH/NH₄OH (9:1:0.1) to give the product as a brownish solid. Yield 94%; mp at 253 °C with decomposition.

¹H NMR (500 MHz, DMSO-*d*₆) δ 8.25 (d, *J* = 2.4 Hz, 1H), 7.64 (d, *J* = 8.9 Hz, 1H), 7.47 (dd, *J* = 8.9, 2.3 Hz, 1H), 6.41 (bs, 2H), 3.01–2.91 (m, 2H), 2.84–2.73 (m, 2H), 1.78 (p, *J* = 5.8 Hz, 2H), 1.61 (p, *J* = 5.5 Hz, 2H), 1.54 (p, *J* = 5.5 Hz, 2H). ¹³C NMR (126 MHz, DMSO-*d*₆) δ 164.83, 146.48, 144.89, 130.54, 128.25, 127.70, 121.62, 118.85, 115.11, 31.74, 27.76, 26.75, 25.50. HRMS (HESI⁺): [M+H]⁺: calculated for C₁₄H₁₆ClN₂⁺ (*m/z*): 247.0997; found: 247.0995. HPLC purity >99%.

5,7-dichloro-1H,2H,3H-cyclopenta[b]quinolin-9-amine hydrochloride (10): 2-amino-3,5-dichlorobenzonitrile (148 mg; 0.79 mmol); AlCl₃ (211 mg; 1.58 mmol). Purified by column chromatography using mobile phase petroleum ether/ethyl acetate (PE/EA) (1:1) to give the product as a brownish solid. Yield 72%; mp at 222 °C with decomposition.

¹H NMR (500 MHz, DMSO-*d*₆) δ 8.27 (d, *J* = 2.3 Hz, 1H), 7.75 (d, *J* = 2.2 Hz, 1H), 6.70 (bs, 2H), 2.93 (t, *J* = 7.7 Hz, 2H), 2.81 (t, *J* = 7.3 Hz, 2H), 2.13–2.02 (m, 2H). ¹³C NMR (126 MHz, DMSO-*d*₆) δ 168.07, 146.26, 143.49, 133.27, 128.02, 126.22, 120.99, 119.31, 115.38, 34.97, 27.86, 22.23. HRMS (HESI⁺): [M+H]⁺: calculated for C₁₂H₁₁Cl₂N₂⁺ (*m/z*): 253.0294; found: 253.0291. HPLC purity >99%.

5,7-dichloro-1,2,3,4-tetrahydroacridin-9-amine hydrochloride (11): 2-amino-3,5-dichlorobenzonitrile (148 mg; 0.79 mmol); AlCl₃ (211 mg; 1.58 mmol). Purified by column chromatography using mobile phase PE/EA (2:1) to give the product as a brownish solid. Yield 86%; mp at 193 °C with decomposition.

¹H NMR (500 MHz, DMSO-*d*₆) δ 8.30 (d, *J* = 2.3 Hz, 1H), 7.74 (d, *J* = 2.2 Hz, 1H), 6.60 (bs, 2H), 2.87–2.82 (m, 2H), 2.53 (t, *J* = 6.0 Hz, 2H), 1.85–1.76 (m, 4H). ¹³C NMR (126 MHz, DMSO-*d*₆) δ 158.97, 148.31, 141.25, 133.08, 128.12, 126.06, 120.83, 118.54, 111.02, 33.97, 23.89, 22.58, 22.38. HRMS (HESI⁺): [M+H]⁺: calculated for C₁₃H₁₃Cl₂N₂⁺ (*m/z*): 267.0450; found: 267.0449. HPLC purity >96%.

2,4-dichloro-6H,7H,8H,9H,10H-cyclohepta[b]quinolin-11-amine hydrochloride (12): 2-amino-3,5-dichlorobenzonitrile (145 mg; 0.775 mmol); AlCl₃ (207 mg; 1.55 mmol). Purified by column chromatography using mobile phase PE/EA (2:1) to give the product as a brownish solid. Yield 96%; mp at 244 °C with decomposition.

¹H NMR (500 MHz, DMSO-*d*₆) δ 8.27 (d, *J* = 2.2 Hz, 1H), 7.75 (d, *J* = 2.2 Hz, 1H), 6.58 (bs, 2H), 3.05–2.96 (m, 2H), 2.84–2.75 (m, 2H), 1.85–1.74 (m, 2H), 1.66–1.58 (m, 2H), 1.58–1.51 (m, 2H). ¹³C NMR (126 MHz, DMSO-*d*₆) δ 165.46, 147.13, 141.05, 133.35, 128.02, 126.71, 121.20, 119.52, 116.09, 39.48, 31.67, 27.52, 26.60, 25.49. HRMS (HESI⁺): [M+H]⁺: calculated for C₁₄H₁₅Cl₂N₂⁺ (*m/z*): 281.0608; found: 281.0604. HPLC purity >99%.

5,7-dibromo-1H,2H,3H-cyclopenta[b]quinolin-9-amine hydrochloride (13): 2-amino-3,5-dibromobenzonitrile (167 mg; 0.605 mmol); AlCl₃ (161 mg; 1.21 mmol). Purified by column chromatography using mobile phase PE/EA (1:1) to give a product as a light orange solid. Yield 82%; mp at 153 °C with decomposition.

¹H NMR (500 MHz, DMSO-*d*₆) δ 8.45 (d, *J* = 2.1 Hz, 1H), 8.01 (d, *J* = 2.1 Hz, 1H), 6.71 (bs, 2H), 2.93 (t, *J* = 7.7 Hz, 2H), 2.82 (t, *J* = 7.3 Hz, 2H), 2.06 (p, *J* = 7.6 Hz, 2H). ¹³C NMR (126 MHz, DMSO-*d*₆) δ 168.38, 146.15, 144.42, 133.59, 125.12, 124.77, 119.79, 115.37, 114.56, 35.03, 27.87, 22.24. HRMS (HESI⁺): [M+H]⁺: calculated for C₁₂H₁₁Br₂N₂⁺ (*m/z*): 342.9263; found: 342.9259. HPLC purity >99%.

5,7-dibromo-1,2,3,4-tetrahydroacridin-9-amine hydrochloride (14): 2-amino-3,5-dibromobenzonitrile (170 mg; 0.616 mmol); AlCl₃ (164 mg; 1.232 mmol). Purified by column chromatography using mobile phase PE/EA (1:1) to give the product as a light orange solid. Yield 55%; mp at 203 °C with decomposition.

¹H NMR (500 MHz, DMSO-*d*₆) δ 8.48 (d, *J* = 2.1 Hz, 2H), 7.99 (d, *J* = 2.0 Hz, 1H), 6.61 (bs, 3H), 2.86–2.80 (m, 2H), 2.55–2.51 (m, 2H), 1.84–1.78 (m, 4H). ¹³C NMR (126 MHz, DMSO-*d*₆) δ 159.27, 148.21, 142.14, 133.66, 125.05, 124.66, 118.99, 114.39, 111.00, 34.01, 23.88, 22.57, 22.38. HRMS (HESI⁺): [M+H]⁺: calculated for C₁₃H₁₃Br₂N₂⁺ (*m/z*): 356.942; found: 356.9414. HPLC purity >97%.

2,4-dibromo-6H,7H,8H,9H,10H-cyclohepta[b]quinolin-11-amine hydrochloride (15): 2-amino-3,5-dibromobenzonitrile (167 mg; 0.605 mmol); AlCl₃ (161 mg; 1.21 mmol). Purified by column chromatography using mobile phase PE/EA (3:1) to give the product as a light orange solid. Yield 65%; mp at 142 °C decomposition.

¹H NMR (500 MHz, DMSO-*d*₆) δ 8.45 (d, *J* = 2.1 Hz, 1H), 8.00 (d, *J* = 1.9 Hz, 1H), 6.60 (bs, 2H), 3.04–2.96 (m, 2H), 2.82–2.76 (m, 2H), 1.83–1.76 (m, 2H), 1.66–1.59 (m, 2H), 1.59–1.51 (m, 2H). ¹³C NMR (126 MHz, DMSO-*d*₆) δ 165.73, 147.06, 141.93, 133.58, 125.26, 125.01, 119.95, 116.06, 115.08, 31.67, 27.53, 26.58, 25.50. HRMS (HESI⁺): [M+H]⁺: calculated for C₁₄H₁₅Br₂N₂⁺ (*m/z*): 370.9576; found: 370.9570. HPLC purity >99%.

7-fluoro-1H,2H,3H-cyclopenta[b]quinolin-9-amine hydrochloride (16): 2-amino-5-fluorobenzonitrile (122 mg; 0.896 mmol); AlCl₃ (239 mg; 1.79 mmol). Purified by column chromatography using mobile phase DCM/MeOH/NH₄OH (9:1:0.1) to give the product as a white solid. Yield 83%; mp at 185 °C with decomposition.

¹H NMR (500 MHz, DMSO-*d*₆) δ 7.97–7.88 (m, 1H), 7.76–7.66 (m, 1H), 7.45–7.31 (m, 1H), 6.40 (bs, 2H), 2.88 (t, *J* = 7.7 Hz, 2H), 2.80 (t, *J* = 7.3 Hz, 2H), 2.05 (p, *J* = 7.5 Hz, 2H). ¹³C NMR (126 MHz, DMSO-*d*₆) δ 166.46, 166.44, 159.10, 157.20, 145.86, 145.84, 130.84, 130.77, 118.05, 117.98, 117.35, 117.15, 113.97, 106.14, 105.96, 34.57, 27.78, 22.43. HRMS (HESI⁺): [M+H]⁺: calculated for C₁₂H₁₂FN₂⁺ (*m/z*): 203.0979; found: 203.0976. HPLC purity >99%.

7-fluoro-1,2,3,4-tetrahydroacridin-9-amine hydrochloride (17): 2-amino-5-fluorobenzonitrile (177 mg; 1.30 mmol); AlCl₃ (347 mg; 2.60 mmol). Purified by column chromatography using mobile phase DCM/MeOH/NH₄OH (9:1:0.1) to give the product as a white solid. Yield 77%; mp at 268 °C with decomposition.

¹H NMR (500 MHz, DMSO-*d*₆) δ 8.08–8.00 (m, 1H), 7.76–7.69 (m, 1H), 7.49–7.41 (m, 1H), 6.75 (bs, 2H), 2.83 (t, *J* = 5.9 Hz, 2H), 2.53 (t, *J* = 6.1 Hz, 2H), 1.85–1.75 (m, 4H). ¹³C NMR (126 MHz, DMSO-*d*₆) δ 159.24, 157.33, 155.97, 149.41, 141.72, 128.92, 118.77, 118.57, 117.06, 109.49, 106.30, 106.12, 32.42, 23.64, 22.32. HRMS (HESI⁺): [M+H]⁺: calculated for C₁₃H₁₄FN₂⁺ (*m/z*): 217.1136; found: 217.1135. HPLC purity >97%.

2-fluoro-6H,7H,8H,9H,10H-cyclohepta[b]quinolin-11-amine hydrochloride (18): 2-amino-5-fluorobenzonitrile (177 mg; 1.30 mmol); AlCl₃ (347 mg; 2.60 mmol). Purified by column chromatography using mobile phase DCM/MeOH/NH₄OH (9:1:0.1) to give the product as a white solid. Yield 98%; mp at 269 °C with decomposition.

¹H NMR (500 MHz, DMSO-*d*₆) δ 7.96–7.89 (m, 1H), 7.71–7.64 (m, 1H), 7.41–7.33 (m, 1H), 6.30 (bs, 2H), 3.01–2.91 (m, 2H), 2.84–2.74 (m, 2H), 1.86–1.74 (m, 2H), 1.65–1.50 (m, 4H). ¹³C NMR (126 MHz, DMSO-*d*₆) δ 160.45, 158.51, 158.05, 153.95, 153.92, 133.87, 122.53, 122.46, 122.15, 121.95, 116.82, 116.74, 114.75, 108.60, 108.40, 32.79, 31.04, 26.23, 25.47, 24.59. HRMS (HESI⁺): [M+H]⁺: calculated for C₁₄H₁₆FN₂⁺ (*m/z*): 231.1292; found: 231.1287. HPLC purity >99%.

8-chloro-1H,2H,3H-cyclopenta[b]quinolin-9-amine hydrochloride (19): 2-amino-6-chlorobenzonitrile (140 mg; 0.92 mmol); AlCl₃ (245 mg; 1.84 mmol). Purified by column chromatography

using mobile phase DCM/MeOH/NH₄OH (15:1:0.1) to give the product as a brownish solid. Yield 63%; mp at 253 °C with decomposition.

¹H NMR (500 MHz, DMSO-*d*₆) δ 7.65 (dd, *J* = 8.4, 1.4 Hz, 1H), 7.41 (dd, *J* = 8.4, 7.5 Hz, 1H), 7.33 (dd, *J* = 7.5, 1.4 Hz, 1H), 6.51 (bs, 2H), 2.90 (t, *J* = 7.8 Hz, 2H), 2.82–2.76 (m, 2H), 2.12–2.02 (m, 2H). ¹³C NMR (126 MHz, DMSO-*d*₆) δ 166.75, 151.22, 146.28, 128.96, 128.27, 127.73, 125.83, 116.29, 114.60, 34.59, 28.15, 22.04. HRMS (HESI⁺): [M+H]⁺: calculated for C₁₂H₁₂ClN₂ (m/z): 219.0684; found: 219.0682. HPLC purity >98%.

8-chloro-1,2,3,4-tetrahydroacridin-9-amine hydrochloride (20): 2-amino-6-chlorobenzonitrile (135 mg; 0.885 mmol); AlCl₃ (236 mg; 1.77 mmol). Purified by column chromatography using mobile phase DCM/MeOH/NH₄OH (15:1:0.1) to give the product as a brownish solid. Yield 48%; mp at 252 °C with decomposition.

¹H NMR (500 MHz, DMSO-*d*₆) δ 7.61 (dd, *J* = 8.4, 1.4 Hz, 1H), 7.44–7.38 (m, 1H), 7.33 (dd, *J* = 7.5, 1.4 Hz, 1H), 6.53 (bs, 2H), 2.80 (t, *J* = 6.2 Hz, 2H), 2.49–2.46 (m, 2H), 1.87–1.75 (m, 4H). ¹³C NMR (126 MHz, DMSO-*d*₆) δ 157.87, 148.60, 148.22, 128.68, 127.82, 127.52, 125.90, 113.89, 111.29, 33.47, 23.98, 22.51, 22.41. HRMS (HESI⁺): [M+H]⁺: calculated for C₁₃H₁₄ClN₂ (m/z): 233.0840; found: 233.0838. HPLC purity >99%.

1-chloro-6H,7H,8H,9H,10H-cyclohepta[b]quinolin-11-amine hydrochloride (21): 2-amino-6-chlorobenzonitrile (135 mg; 0.885 mmol); AlCl₃ (236 mg; 1.77 mmol). Purified by column chromatography using mobile phase DCM/MeOH/NH₄OH (15:1:0.1) to give the product as a brownish solid. Yield 89%; mp at 244 °C with decomposition.

¹H NMR (500 MHz, DMSO-*d*₆) δ 7.62 (s, 1H), 7.44–7.38 (m, 1H), 7.35 (dd, *J* = 7.5, 1.5 Hz, 1H), 6.59 (bs, 2H), 2.99–2.92 (m, 2H), 2.81–2.72 (m, 2H), 1.79 (t, *J* = 5.7 Hz, 2H), 1.65–1.52 (m, 4H). ¹³C NMR (126 MHz, DMSO-*d*₆) δ 164.40, 148.64, 147.14, 129.09, 127.78, 127.76, 126.57, 116.44, 114.79, 39.01, 31.57, 27.37, 26.61, 25.35. HRMS (HESI⁺): [M+H]⁺: calculated for C₁₄H₁₆ClN₂ (m/z): 247.0997; found: 247.0994. HPLC purity >98%.

6-methyl-1H,2H,3H-cyclopenta[b]quinolin-9-amine hydrochloride (22): 2-amino-4-methylbenzonitrile (148 mg; 1.12 mmol); AlCl₃ (299 mg; 2.24 mmol). Purified by column chromatography using mobile phase DCM/MeOH/NH₄OH (9:1:0.1) to give the product as a brownish solid. Yield 83%; mp at 273 °C with decomposition.

¹H NMR (500 MHz, DMSO-*d*₆) δ 8.02 (d, *J* = 8.5 Hz, 1H), 7.45 (t, *J* = 1.4 Hz, 1H), 7.14 (dd, *J* = 8.5, 1.8 Hz, 1H), 6.49 (bs, 2H), 2.87 (t, *J* = 7.7 Hz, 2H), 2.78 (t, *J* = 7.4 Hz, 2H), 2.41 (s, 3H), 2.10–1.99 (m, 2H). ¹³C NMR (126 MHz, DMSO-*d*₆) δ 166.02, 148.26, 146.68, 137.59, 126.95, 124.87, 122.10, 115.56, 112.98, 34.53, 27.73, 22.40, 21.33. HRMS (HESI⁺): [M+H]⁺: calculated for C₁₃H₁₅N₂ (m/z): 199.123; found: 199.1228. HPLC purity >99%.

6-methyl-1,2,3,4-tetrahydroacridin-9-amine hydrochloride (23): 2-amino-4-methylbenzonitrile (142 mg; 1.07 mmol); AlCl₃ (287 mg; 2.15 mmol). Purified by column chromatography using mobile phase DCM/MeOH/NH₄OH (9:1:0.1) to give the product as a brownish solid. Yield 77%; mp at 225 °C with decomposition.

¹H NMR (500 MHz, DMSO-*d*₆) δ 8.04 (d, *J* = 8.6 Hz, 1H), 7.43–7.38 (m, 1H), 7.12 (dd, *J* = 8.5, 1.8 Hz, 1H), 6.36 (bs, 2H), 2.80 (t, *J* = 6.0 Hz, 2H), 2.52 (t, *J* = 6.1 Hz, 2H), 2.40 (s, 3H), 1.85–1.74 (m, 4H). ¹³C NMR (126 MHz, DMSO-*d*₆) δ 157.03, 148.53, 146.22, 137.63, 126.58, 124.89, 121.97, 115.09, 108.51, 33.41, 23.69, 22.75, 22.68, 21.37. HRMS (HESI⁺): [M+H]⁺: calculated for C₁₄H₁₇N₂ (m/z): 213.1386; found: 213.1384. HPLC purity >98%.

3-methyl-6H,7H,8H,9H,10H-cyclohepta[b]quinolin-11-amine hydrochloride (24): 2-amino-4-methylbenzonitrile (142 mg; 1.07 mmol); AlCl₃ (287 mg; 2.15 mmol). Purified by column chromatography using mobile phase DCM/MeOH/NH₄OH (5:1:0.1) to give the product as a brownish solid. Yield 99%; mp at 274 °C with

decomposition.

¹H NMR (500 MHz, DMSO-*d*₆) δ 8.08 (d, *J* = 8.5 Hz, 1H), 7.52–7.44 (m, 1H), 7.20 (dd, *J* = 8.5, 1.8 Hz, 1H), 6.75 (bs, 2H), 3.02–2.95 (m, 2H), 2.83–2.74 (m, 2H), 2.42 (s, 3H), 1.79 (p, *J* = 5.9 Hz, 2H), 1.62 (p, *J* = 5.5 Hz, 2H), 1.55 (p, *J* = 5.7 Hz, 2H). ¹³C NMR (126 MHz, DMSO-*d*₆) δ 162.56, 148.75, 144.21, 138.65, 125.84, 125.29, 122.57, 115.46, 113.79, 37.84, 31.67, 27.57, 26.55, 25.22, 21.32. HRMS (HESI⁺): [M+H]⁺: calculated for C₁₅H₁₉N₂ (m/z): 227.1543; found: 227.154. HPLC purity >99%.

8-methyl-1H,2H,3H-cyclopenta[b]quinolin-9-amine hydrochloride (25): 2-amino-6-methylbenzonitrile (158 mg; 1.196 mmol); AlCl₃ (319 mg; 2.39 mmol). Purified by column chromatography using mobile phase DCM/MeOH/NH₄OH (5:1:0.1) to give the product as a yellowish solid. Yield 58%; mp at 275 °C with decomposition.

¹H NMR (500 MHz, DMSO-*d*₆) δ 7.51 (dd, *J* = 8.4, 1.4 Hz, 1H), 7.31 (dd, *J* = 8.4, 7.0 Hz, 1H), 7.02 (d, *J* = 7.0 Hz, 1H), 5.88 (bs, 2H), 2.92–2.85 (m, 5H), 2.79 (t, *J* = 7.3 Hz, 2H), 2.05 (p, *J* = 7.6 Hz, 2H). ¹³C NMR (126 MHz, DMSO-*d*₆) δ 165.19, 150.22, 148.36, 134.19, 127.49, 126.91, 126.24, 117.92, 115.72, 34.36, 28.03, 24.24, 22.20. HRMS (HESI⁺): [M+H]⁺: calculated for C₁₃H₁₅N₂ (m/z): 199.123; found: 199.1227. HPLC purity >99%.

8-methyl-1,2,3,4-tetrahydroacridin-9-amine hydrochloride (26): 2-amino-6-methylbenzonitrile (160 mg; 1.21 mmol); AlCl₃ (323 mg; 2.42 mmol). Purified by column chromatography using mobile phase DCM/MeOH/NH₄OH (9:1:0.1) to give the product as a yellowish solid. Yield 77%; mp at 240 °C with decomposition.

¹H NMR (500 MHz, CD₃OD) δ 7.57–7.53 (m, 1H), 7.50–7.45 (m, 1H), 7.20–7.16 (m, 1H), 2.94 (s, 3H), 2.90 (t, *J* = 6.2 Hz, 2H), 2.55 (t, *J* = 6.3 Hz, 2H), 1.99–1.87 (m, 4H). ¹³C NMR (126 MHz, CD₃OD) δ 155.34, 155.06, 145.15, 135.86, 131.20, 128.97, 122.86, 117.54, 111.72, 31.63, 24.31, 24.27, 23.40, 22.91. HRMS (HESI⁺): [M+H]⁺: calculated for C₁₄H₁₇N₂ (m/z): 213.1386; found: 213.1384. HPLC purity >95%.

1-methyl-6H,7H,8H,9H,10H-cyclohepta[b]quinolin-11-amine hydrochloride (27): 2-amino-6-methylbenzonitrile (160 mg; 1.121 mmol); AlCl₃ (323 mg; 2.42 mmol). Purified by column chromatography using mobile phase DCM/MeOH/NH₄OH (7:1:0.1) to give the product as a yellowish solid. Yield 59%; mp at 235 °C with decomposition.

¹H NMR (500 MHz, DMSO-*d*₆) δ 7.50 (dd, *J* = 8.3, 1.4 Hz, 1H), 7.34 (dd, *J* = 8.4, 7.0 Hz, 1H), 7.07 (dt, *J* = 7.0, 1.2 Hz, 1H), 6.04 (bs, 2H), 3.00–2.93 (m, 2H), 2.89 (s, 3H), 2.81–2.74 (m, 2H), 1.83–1.76 (m, 2H), 1.63 (p, *J* = 5.7, 5.3 Hz, 2H), 1.56 (p, *J* = 5.7 Hz, 2H). ¹³C NMR (126 MHz, DMSO-*d*₆) δ 162.27, 149.90, 146.76, 134.00, 127.93, 127.16, 125.97, 118.22, 115.87, 38.19, 31.60, 27.54, 26.62, 25.21, 24.26. HRMS (HESI⁺): [M+H]⁺: calculated for C₁₅H₁₉N₂ (m/z): 227.1543; found: 227.1539. HPLC purity >99%.

7-methoxy-1H,2H,3H-cyclopenta[b]quinolin-9-amine hydrochloride (28): 2-amino-5-methoxybenzonitrile (177 mg; 1.19 mmol); AlCl₃ (319 mg; 2.39 mmol). Purified by column chromatography using mobile phase DCM/MeOH/NH₄OH (9:1:0.1) to give the product as a white solid. Yield 60%; mp at 264 °C with decomposition.

¹H NMR (500 MHz, DMSO-*d*₆) δ 7.59 (d, *J* = 9.1 Hz, 1H), 7.49 (d, *J* = 2.8 Hz, 1H), 7.14 (dd, *J* = 9.1, 2.7 Hz, 1H), 6.30 (bs, 2H), 3.85 (s, 3H), 2.86 (t, *J* = 7.7 Hz, 2H), 2.80 (t, *J* = 7.3 Hz, 2H), 2.10–1.99 (m, 2H). ¹³C NMR (126 MHz, DMSO-*d*₆) δ 164.15, 155.28, 145.52, 144.07, 129.58, 119.44, 118.05, 113.64, 101.55, 55.67, 34.35, 27.79, 22.50. HRMS (HESI⁺): [M+H]⁺: calculated for C₁₃H₁₅ON₂ (m/z): 215.1179; found: 215.1176. HPLC purity >99%.

7-methoxy-1,2,3,4-tetrahydroacridin-9-amine hydrochloride (29): 2-amino-5-methoxybenzonitrile (181 mg; 1.24 mmol); AlCl₃ (330 mg; 2.48 mmol). Purified by column chromatography using mobile phase DCM/MeOH/NH₄OH (9:1:0.1) to give the product as a yellowish solid. Yield 52%; mp 163 °C.

^1H NMR (500 MHz, $\text{DMSO}-d_6$) δ 7.60–7.53 (m, 2H), 7.20 (dd, $J = 9.1, 2.7$ Hz, 1H), 6.56 (bs, 2H), 3.86 (s, 3H), 2.81 (t, $J = 6.0$ Hz, 2H), 2.54 (t, $J = 6.2$ Hz, 2H), 1.85–1.76 (m, 4H). ^{13}C NMR (126 MHz, $\text{DMSO}-d_6$) δ 155.54, 154.03, 148.65, 140.37, 127.96, 120.80, 117.21, 109.12, 101.28, 55.80, 32.42, 23.71, 22.50. HRMS (HESI^+): $[\text{M}+\text{H}]^+$: calculated for $\text{C}_{14}\text{H}_{17}\text{ON}_2^+$ (m/z): 229.1335; found: 229.1331. HPLC purity >97%.

2-methoxy-6H,7H,8H,9H,10H-cyclohepta[b]quinolin-11-amine hydrochloride (30): 2-amino-5-methoxybenzonitrile (181 mg; 1.24 mmol); AlCl_3 (330 mg; 2.48 mmol). Purified by column chromatography using mobile phase $\text{DCM}/\text{MeOH}/\text{NH}_4\text{OH}$ (7:1:0.1) to give the product as a yellowish solid. Yield 82%; mp 237 °C.

^1H NMR (500 MHz, $\text{DMSO}-d_6$) δ 7.64 (d, $J = 9.1$ Hz, 1H), 7.56 (d, $J = 2.7$ Hz, 1H), 7.23 (dd, $J = 9.1, 2.6$ Hz, 1H), 6.75 (bs, 2H), 3.87 (s, 3H), 3.02–2.94 (m, 2H), 2.85–2.77 (m, 2H), 1.80 (p, $J = 5.9$ Hz, 2H), 1.63 (p, $J = 5.4$ Hz, 2H), 1.57 (p, $J = 5.5$ Hz, 2H). ^{13}C NMR (126 MHz, $\text{DMSO}-d_6$) δ 160.14, 156.15, 156.15, 148.24, 139.03, 127.41, 120.78, 117.96, 114.38, 102.09, 55.91, 37.46, 31.62, 27.51, 26.56, 25.35. HRMS (HESI^+): $[\text{M}+\text{H}]^+$: calculated for $\text{C}_{14}\text{H}_{17}\text{ON}_2^+$ (m/z): 243.1492; found: 243.1488. HPLC purity >99%.

5.3. In vitro anti-cholinesterase assay

The inhibitory activity of 7-PhO-THA and all the standards against human recombinant AChE (hAChE, E.C. 3.1.1.7, purchased from Sigma-Aldrich, Prague, Czech Republic) and human plasmatic butyrylcholinesterase (hBChE, E.C. 3.1.1.8, purchased from Sigma-Aldrich, Prague, Czech Republic) were determined using the modified Ellman's method [31], according to previously published protocol [54]. The results are expressed as IC_{50} values (the concentration of the compound that is required to reduce 50% of cholinesterase (ChE) activity). For calculation of the percentage inhibition of activity (I) the following equation 1 was used:

$$I = \left(1 - \frac{\Delta A_i}{\Delta A_0}\right) \times 100 \text{ [\%]} \quad (1)$$

where ΔA_i indicates the absorbance change provided by adequate enzyme exposed to its corresponding inhibitor, and ΔA_0 indicates the absorbance change when a solution of PBS was added instead of a solution of inhibitor. Software Microsoft Excel 10 (Microsoft Corporation, Redmont, WA, USA) and GraphPad Prism version 5.02 for Windows (GraphPad Software, San Diego, CA, USA) were used for evaluation of the statistical data.

5.4. The cell culture and transfection with DNA vectors

The DNA vectors encoding the human versions of GluN1-1a (GluN1), GluN2A and GluN2B subunits as well as green fluorescent protein (GFP) have been described recently [55]. Human embryonic kidney 293 (HEK293) cells were cultured in Opti-MEM I media containing 5% fetal bovine serum (FBS; v/v; Thermo Fisher Scientific). The HEK293 cells were transfected in Opti-MEM I media containing a mixture of 0.6 μL of MATra-A Reagent (IBA) and 600 ng of DNA vectors carrying the GluN1, GluN2 and GFP (diluted in equal ratio), and were then placed on a magnet plate for 30 min [56]. After that, the HEK293 cells were trypsinised and grown in Opti-MEM I containing 1% FBS, 20 mM MgCl_2 and 3 mM kynurenic acid (to reduce excitotoxicity) on 35 mm glass coverslips. Electrophysiological recordings were performed at room temperature within 24–48 h after transfection.

5.5. Electrophysiology

Whole-cell patch-clamp recordings were performed using Axopatch 200B amplifiers (Molecular Devices), combined with WASO2 application systems [15,57]. The extracellular recording solution (ECS) had the following composition (in mM): 160 NaCl, 2.5 KCl, 10 HEPES, 10 glucose, 0.2 EDTA, and 0.7 CaCl_2 (pH adjusted to 7.3 with NaOH). In all experiments, the ECS contained the saturating concentration of co-agonist glycine (50 μM) and the NMDARs were activated by the saturating concentration of agonist glutamate (1 mM; Merck). The stock solutions of 7-MEOTA and its derivatives (10 mM) were prepared freshly before each experiment in dimethyl sulfoxide (DMSO; Merck) [15]. Glass pipettes with 5–7 M Ω tip resistance made using a P-1000 horizontal puller (Sutter Instrument Co.) were filled with the intracellular recording solution containing (in mM): 125 gluconic acid, 15 CsCl, 5 EGTA, 10 HEPES, 3 MgCl_2 , 0.5 CaCl_2 , and 2 ATP-Mg salt (pH adjusted to 7.2 with CsOH). The currents were filtered at 2 kHz with an eight-pole low-pass Bessel filter and digitized at 5 kHz with Digidata 1322A digitizers and pClamp 10 software (Molecular Devices). All recordings were performed at the indicated holding potentials (–60 or +40 mV). The dose-response inhibitory curves for 7-MEOTA and its derivatives were obtained using Equation (2).

$$I = 1 / (1 + ([\text{compound}] / \text{IC}_{50})^h) \quad (2)$$

where IC_{50} is the concentration of tested compound that produces a 50% inhibition of agonist-evoked current, [compound] is the concentration of tested compounds, and h is the apparent Hill coefficient.

5.6. Quantitative structure activity relationship (QSAR)

Partial least squares projection to latent structures (PLS) analysis [58] was carried out for exploration of the relationships between the molecular and structural descriptors (X) and experimentally determined inhibitory activity towards NMDARs consisting of the GluN2A or GluN2B subunit respectively (y). Molecular and structure descriptors were calculated using the software tool MORDRED (Osaka University, Japan, <https://mordred.phs.osaka-u.ac.jp/>) [37]. PLS uses the correlation structure among the original variables and the variables are weighted together by the PLS weights to a small number of new latent variables. Auto-scaled and centered data were used in the PLS analysis. The importance of every descriptor in the model was accessed using the variable importance in the projection (VIP) parameter [59] and scores plots and loadings plots [60]. Validation was employed to assess the quality and validity of developed PLS models [61]. The validation was secured by a cross-validation routine and permutation testing. During the cross-validation procedure [59], parts of the y data are kept out of model development and predicted by the model, and compared with the actual values, providing cross-validated Q^2 . This gives a more realistic value for the predictive power than the squared multiple regression coefficient R^2 . In this study 1/7 of the compounds were deleted at each cross-validation round. In the permutation testing, the model is recalculated 999-times using a randomly re-ordered dependent variable. The statistical package SIMCA-P version 12 (Umetrics, Umea, Sweden) was used for statistical analyses.

5.7. Blood-brain barrier permeability prediction

The MDCK assay evaluates the ability of compounds to diffuse from the donor compartment through the MDCK's cell membrane into the acceptor compartment. The MDCK cells were seeded on a

polycarbonate membrane (area 1.12 cm²) with 3 µm pores of the 12-well plates with 12 mm inserts. The tested compounds were dissolved in DMSO and then diluted with OptiMEM to reach the final concentrations (in the range 100 µM); the concentration of DMSO did not exceed 0.5% (v/v). 750 µL of the donor solution was added to the donor compartment (insert) and the same volume of OptiMEM was added into the acceptor. The concentration of the drug in both compartments was measured in triplicate by UV-VIS spectrophotometry after 1, 2, 4 and 6 h of incubation. The apparent permeability coefficient (*P_{app}*) was calculated from the concentrations ratio using equation (3). The tightness of the MDCK monolayer is assessed by the permeability of FITC (fluorescein isothiocyanate) at 0.4 mg/mL.

$$P_{app} = \frac{dC}{dt} \cdot \frac{V_r}{A \cdot C_0} \quad (3)$$

where, A is area of the well/cell monolayer.

dC/dt is amount in the receiver compartment in given time
V_r is volume of the receiver compartment
C₀ is the initial concentration of tested compounds

5.8. In vivo pharmacokinetic study

5.8.1. Animals

Adult male ICR mice (23–25 g) purchased from the Velaz breeding colony were used. The mice were housed in transparent plastic boxes in an air-conditioned animal room of Faculty of Military Health Sciences, Hradec Kralove, Czech Republic. The mice were kept under a 12:12 h light/dark cycle, with free access to food and water. All experiments were performed after a week-long acclimatization period. The experiments were conducted in accordance with the guidelines of the European Union directive 2010/63/EU and Act No246/1992 Coll. The handling of the experimental animals was done under the supervision of the Ethics Committee of the Faculty of Military Health Sciences, Czech Republic.

40 male mice (20–30 g, Velaz Ltd., Czech Republic) were injected i.p. with the tested compounds at a concentration of 5 mg kg⁻¹ in 5% DMSO/saline mixture. Blood samples were collected under deep terminal anesthesia directly by cardiac puncture into heparinized 1.5 mL tubes at 15 and 60 min (3 animals per time interval). Four animals were used for zero time or blank control. The animals were perfused transcardially with saline solution (0.9% NaCl) for 5 min (1 mL/min) [62], and after the wash-out the skull was opened, and the brain carefully removed; brains were stored at –80 °C until analysis.

The brains were weighed PBS was added in the weight ratio 1:4. The brains were subsequently homogenised by T-25 Ultra Turrax disperser (IKA, Staufen, Germany), ultrasonicated by UP 50H needle homogeniser (Hielscher, Teltow, Germany), and stored at –80 °C prior to extraction.

5.8.2. Sample extraction

190 µL of brain homogenate or 95 µL of plasma was spiked with 10 µL (homogenate) or 5 µL (plasma) of internal standard (IS; 7-PhO-THA in methanol), so that the final concentration was 1 µM, the sample alkalinized with 100 µL of 1 M sodium hydroxide, and 1000 µL of ethyl acetate was added. The samples were then vortexed (1200 RPM, Wizard Advanced IR Vortex Mixer, Velp Scientifica, Usmate, Italy) and centrifuged (12000 RPM, 5 min, Universal 320 R centrifuge, Hettich, Tuttlingen, Germany). 700 µL of supernatant was transferred to a microtube and evaporated to dryness in a CentriVap concentrator (Labconco Corporation, Kansas City, USA).

Calibration samples were prepared by spiking 90 µL of blank plasma or 180 µL of blank brain homogenate with 5 µL (plasma) or 10 µL (homogenate) of the studied compounds dissolved in methanol (final concentrations range from 0.5 nM to 50 µM) and 5 or 10 µL of IS (7-PhO-THA in methanol, final concentration 1 µM), and then vortexing and extracting as above. Analysis samples were reconstituted in 100 µL of acetonitrile/water mixture 50/50 (v/v).

5.8.3. Liquid chromatography mass spectrometry

Solvents and other common chemicals were purchased from VWR (Stribrna Skalice, Czech Republic). Solvents for chromatographic procedures were supplied in LC-MS grade. 7-phenoxycacrine (7-PhO-THA) was synthesized *de novo* and used as the internal standard.

5.8.4. HPLC-MS instrumentation

The system used in this study was Dionex Ultimate 3000 UHPLC RS consisting of RS Pump, RS Column Compartment, RS Autosampler and Diode Array Detector controlled by Chromeleon (version 7.2.9. build 11323) software (Thermo Fisher Scientific, Germering, Germany) with Q Exactive Plus Orbitrap mass spectrometer with Thermo Xcalibur (version 3.1.66.10.) software (Thermo Fisher Scientific, Bremen, Germany). Detection was performed by mass spectrometry in positive mode. Settings of the heated electrospray source were: spray voltage 3.5 kV; capillary temperature 220 °C; sheath gas 55 arbitrary units; auxiliary gas 15 arbitrary units; spare gas 3 arbitrary units; probe heater temperature 220 °C; max spray current 100 µA; S-lens RF Level 50.

5.8.5. High-resolution mass spectrometry and purity

HRMS and sample purities were obtained by high performance liquid chromatography (HPLC) with the UV and mass spectrometry gradient method. A C18 column (Waters Atlantis dC18; 2.1 × 100mm; 3 µm, Waters, Wexford, Ireland) was used in this study. Mobile phase A was ultrapure water of ASTM I type (resistance 18.2 MΩ cm at 25 °C) prepared by Barnstead Smart2Pure 3 UV/UF apparatus (Thermo Fisher Scientific, Bremen, Germany) with 0.1% (v/v) formic acid; mobile phase B was acetonitrile with 0.1% (v/v) of formic acid. The flow was constant at 0.4 mL/min. The method started with 1 min of isocratic flow of 5% B, the concentration of B was then increased to 100% in 15 min and remained constant at 100% B for 1 min. The composition then reverted to 5% B and equilibrated for 5.5 min. The column was tempered to 27 °C. Samples were dissolved in methanol at a concentration of 1 mg/mL and sample injection was 1 µL. Purity was determined from UV spectra measured at wavelength 254 nm. HRMS was determined in total ion current spectra from the mass spectrometer in positive mode.

5.8.6. Pharmacokinetic study - HPLC-MS analysis

Compound levels in plasma and brain homogenate were measured by the above-mentioned UHPLC system with mass spectrometric detection. The results were obtained by gradient elution with reverse phase on a C18 column (Luna Omega Polar C18, 2.1 × 50 mm, 1.6 µm, Phenomenex, Torrance, California, USA) with SecurityGuard ULTRA Cartridge (C18, 2.1 µm, Phenomenex, Torrance, California, USA). The mobile phase was as above: water and acetonitrile with formic acid. Initially 5% B flowed for 0.2 min, and the composition then increased to 100% B in 3 min. After 0.5 min steady flow of 100% B the composition reverted to 5% B and equilibrated for 1.8 min. The total run time of the method was 5.5 min. Flow of the mobile phase was set to 0.5 mL/min and the column was tempered to 40 °C. The injection volume was 5 µL. Samples were analyzed by the previously-mentioned Orbitrap mass spectrometer in parallel reaction monitoring (PRM) positive

mode. Settings for each compound and internal standard are in Table 4. The calibration curves had 6 points, and for brain homogenates ranged from 5 nM to 1 µM and for plasma samples from 50 nM to 10 µM, and were linear in the measured range.

5.9. Behavioral experiments

5.9.1. Animals

Adult male Wistar rats (280–400 g, 2–3 months) purchased from the Velaz breeding colony were used. The rats were housed in pairs in transparent plastic boxes (50 × 25 × 25 cm) in an air-conditioned animal room of National Institute of Mental Health, Prague, Czech Republic. The rats were kept under a 12:12 h light/dark cycle, with free access to food and water. All experiments were performed in the light phase of the day after a week-long acclimatization period. The experiments were conducted in accordance with the guidelines of European Union directive 2010/63/EU and Act No. 246/1992 Coll. on the protection of animals against cruelty, and were approved by the Animal Care and Use Committee of the National Institute of Mental Health (reference number MZDR 51755/2018-4/OVZ).

5.9.2. Drugs

The rats were pseudo-randomly assigned to 16 experimental groups according to treatment: DMSO (control for the 1 mg/kg groups), **4** (1 mg/kg), **5** (1 mg/kg), **7** (1 mg/kg), **21** (1 mg/kg), **23** (1 mg/kg), **28** (1 mg/kg), DMSO (control for the 5 mg/kg groups), **4** (5 mg/kg), **5** (5 mg/kg), **7** (5 mg/kg), **21** (5 mg/kg), **23** (5 mg/kg), **28** (5 mg/kg), 7-MEOTA (5 mg/kg) and MK-801. The compounds were administered intraperitoneally 15 min before the behavioral testing, except for the comparator drugs MK-801 and 7-MEOTA, which were administered 30 min before the testing, based on our previous study [15]. For application of the compounds at a dose of 1 mg/kg, the compounds **5**, **7**, **21**, **23** and **28** were dissolved in a vehicle consisting of 5% dimethyl sulfoxide (DMSO) in physiological saline (drug concentration 1 mg/mL of vehicle) and administered at an injection volume of 1 mL/kg. For the dose of 5 mg/kg, the compounds **5**, **7**, **21**, **23**, **28** and 7-MEOTA were dissolved in the same vehicle (2 mg/mL of the vehicle) and then administered at an injection volume of 2.5 mL/kg. MK-801 ((+)-MK-801 hydrogen maleate, Sigma-Aldrich) was dissolved in the same vehicle and administered at an injection volume also of 2.5 mL/kg; the dose of MK-801 was 0.2 mg/kg for the open field and 0.3 mg/kg for the PPI experiment. Due to the suboptimal solubility of compound **4**, the solution vehicle for this contained the corresponding volume of distilled water instead of saline. Gentle heating was used during preparation of the solutions. Control animals (DMSO groups) received corresponding volumes of the vehicle (1 or 2.5 mL/kg).

5.9.3. Open field

The effect of the compounds on spontaneous locomotor activity in the open field was assessed. The experiments were performed in

a black plastic square arena (80 × 80 cm), located in a separate room with defined light conditions (80 lx). The rat was placed in the center of the arena and then recorded for 10 min by a camera placed above the arena, connected to tracking software (EthoVision 14, Noldus, Netherlands). The arena was thoroughly cleaned between the animals. The dependent variable was the distance moved by the animal. The number of animals was 8 in the DMSO group (control for the 1 mg/kg groups; 1 mL/kg), 8 in MK-801 group and 6 in each other group.

5.9.4. Prepulse inhibition of acoustic startle response (PPI)

Next, the effect of the compounds on prepulse inhibition of acoustic startle response was tested. The experimental design was as previously described in Ref. [15].

The apparatus (SR-LAB, San Diego Instruments, CA, USA) consisted of a soundproof chamber, a piezoelectric accelerometer, a cylinder for animal placement and a loudspeaker. The animal was placed in a plexiglass cylinder (9 cm diameter, 17 cm length). The amplitudes of the startle response were detected by a piezoelectric accelerometer mounted below the cylinders and further analyzed. The background noise was set at 75 dB for the entire experiment. Habituation took place two days before the test session. Drug-free animals were exposed to 6 pulse stimuli alone (125 dB/40 ms) over white background noise after a 5-min acclimatization period. For the test sessions, the drug was administered to the animals 15 min before the test. After the 5-min acclimatization period the session began with 72 trials with variable inter-trial interval (ITI) of 4–20 s (mean ITI 12.27 s). Automatically randomized durations of ITIs ensured that the animal would not discern a pattern that could skew results. First, six pulse stimuli alone (125 dB/40 ms) were presented. Subsequently, 60 trials were presented in pseudo-random order: A) pulse alone 40 ms 125 dB; B) prepulse-pulse: 20 ms of two different intensities of prepulses 83 dB or 91 dB with a variable (30, 60 or 120 ms) inter-stimulus interval followed by a 125 dB pulse of 40 ms duration; C) no stimulus (60 ms). Finally, six pulse stimuli alone (125 dB/40 ms) were delivered again. PPI was calculated as the difference between the average values of the single pulse and prepulse-pulse trials and it was expressed as a percentage of PPI:

$$100 - (\text{mean response to prepulse-pulse trials} / \text{mean startle response to pulse alone trials}) * 100$$

The number of animals was 8 in the groups DMSO (control for the 5 mg/kg groups; 2.5 mL/kg), **28** 1 mg/kg, and **21** 5 mg/kg; and 6 animals in other groups.

5.9.5. Statistics

The data from open field (distance moved) and PPI (% PPI) were subjected to the following analyses in GraphPad Prism 8 (San Diego, USA). First, the data from each group was tested for outliers using Grubb's test. The tests detected two outliers in distance moved in

Table 4
Parameters for HPLC-MS analysis.

Compound	Parent ion	Normalised collision energy	Selected product ion	t _R (min)
4	263.01816	70	216.08891	2.70
5	277.03339	70	249.00175	2.80
7	219.06799	70	167.07271	2.65
21	247.09894	70	206.05989	2.85
23	213.13795	70	185.10680	2.75
28	215.11729	70	172.09897	2.65
7-PhO-THA (IS)	291.14853	70	230.10452	3.15

t_R, retention time; IS, internal standard.

open field (in groups **21** 5 mg/kg and 7-MEOTA 5 mg/kg) and one in % PPI (**21** 5 mg/kg). The outliers were excluded from further analyses. The data was evaluated using ANOVA (the effects of the drugs at a dose of 1 and 5 mg/kg analyzed separately), followed by Bonferroni's multiple comparisons test when appropriate. The data from open field (5 mg/kg doses) did not meet the assumption of homogeneity of variances for ANOVA (Bartlett's test), therefore Brown-Forsythe ANOVA with Dunnett's T3 multiple comparison test was used. The differences were considered significant at $P < 0.05$. The graphs show group means \pm S.E.M.; asterisks denote significant difference from the corresponding control group (DMSO): * $P < 0.05$, ** $P < 0.01$, *** $P < 0.001$ and **** $P < 0.0001$.

Declaration of interest

The authors declare that they have no known competing financial interests or personal relationships that could have appeared to influence the work reported in this paper.

Declaration of competing interest

The authors declare that they have no known competing financial interests or personal relationships that could have appeared to influence the work reported in this paper.

Acknowledgements

Authors would like to thank the grant of Czech Science Foundation (no. 20-12047S, M.H.) to project TACR (no. TO01000078 O.S.) and European Regional Development Fund: Project "PharmaBrain" (no. CZ.CZ.02.1.01/0.0/0.0/16_025/0007444; K.V.) and Charles University (SVV 260547; M.N.). The authors are grateful to Jana Hatlapatkova for animal handling and Ian McColl MD, PhD for assistance with the manuscript.

Appendix A. Supplementary data

Supplementary data to this article can be found online at <https://doi.org/10.1016/j.ejmech.2021.113434>.

References

- [1] R. Morphy, C. Kay, Z. Rankovic, From magic bullets to designed multiple ligands, *Drug Discov. Today* 9 (2004) 641–651.
- [2] E. Proschak, H. Stark, D. Merk, Polypharmacology by design: a medicinal chemist's perspective on multitargeting compounds, *J. Med. Chem.* 62 (2018) 420–444.
- [3] C. Albertini, A. Salerno, P. de Sena Murteira Pinheiro, M.L. Bolognesi, From combinations to multitarget-directed ligands: a continuum in Alzheimer's disease polypharmacology, *Med. Res. Rev.* (2020), <https://doi.org/10.1002/med.21699>.
- [4] R. Morphy, Z. Rankovic, Designed multiple ligands. An emerging drug discovery paradigm, *J. Med. Chem.* 48 (2005) 6523–6543.
- [5] O. Benek, J. Korabecny, O. Soukup, A perspective on multi-target drugs for Alzheimer's disease, *Trends Pharmacol. Sci.* 41 (2020) 434–445.
- [6] A. Calhoun, C. King, R. Khoury, G.T. Grossberg, An evaluation of memantine ER+ donepezil for the treatment of Alzheimer's disease, *Expert Opin. Pharmacother.* 19 (2018) 1711–1717.
- [7] E. Simoni, S. Daniele, G. Bottegioni, D. Pizzirani, M.L. Trincavelli, L. Goldoni, G. Tarozzo, A. Reggiani, C. Martini, D. Piomelli, Combining galantamine and memantine in multitargeted, new chemical entities potentially useful in Alzheimer's disease, *J. Med. Chem.* 55 (2012) 9708–9721.
- [8] A.M. Reggiani, E. Simoni, R. Caporaso, J. Meunier, E. Keller, T. Maurice, A. Minarini, M. Rosini, A. Cavalli, In vivo characterization of ARN14140, a memantine/galantamine-based multi-target compound for Alzheimer's disease, *Sci. Rep.* 6 (2016) 1–11.
- [9] Z. Gazova, O. Soukup, V. Sepsova, K. Siposova, L. Drtinova, P. Jost, K. Spilovska, J. Korabecny, E. Nepovimova, D. Fedunova, M. Horak, M. Kaniakova, Z.J. Wang, A.K. Hamouda, K. Kuca, Multi-target-directed therapeutic potential of 7-methoxytacrine-adamantylamine heterodimers in the Alzheimer's disease treatment, *Biochim. Biophys. Acta (BBA) - Mol. Basis Dis.* 1863 (2017) 607–619.
- [10] K. Spilovska, J. Korabecny, J. Kral, A. Horova, K. Musilek, O. Soukup, L. Drtinova, Z. Gazova, K. Siposova, K. Kuca, 7-Methoxytacrine-Adamantylamine heterodimers as cholinesterase inhibitors in Alzheimer's disease treatment — synthesis, biological evaluation and molecular modeling studies, *Molecules* (2013) 2397–2418.
- [11] M. Kaniakova, E. Nepovimova, L. Kleteckova, K. Skrenkova, K. Holubova, Z. Chrienova, V. Hepnarova, T. Kucera, T. Kobrlova, K. Vales, Combination of memantine and 6-chlorotacrine as novel multi-target compound against Alzheimer's disease, *Curr. Alzheimer Res.* 16 (2019) 821–833.
- [12] J.-M. Zhang, G.-Y. Hu, Huperzine A, a nootropic alkaloid, inhibits N-methyl-D-aspartate-induced current in rat dissociated hippocampal neurons, *Neuroscience* 105 (2001) 663–669.
- [13] Y.W. Liu, C.Y. Li, J.L. Luo, W.M. Li, H.J. Fu, Y.Z. Lao, L.J. Liu, Y.P. Pang, D.C. Chang, Z.W. Li, R.W. Peoples, Y.X. Ai, Y.F. Han, Bis(7)-tacrine prevents glutamate-induced excitotoxicity more potently than memantine by selectively inhibiting NMDA receptors, *Biochem. Biophys. Res. Commun.* 369 (2008) 1007–1011.
- [14] M. Horak, K. Holubova, E. Nepovimova, J. Krusek, M. Kaniakova, J. Korabecny, L. Vyklicky, K. Kuca, A. Stuchlik, J. Ricny, K. Vales, O. Soukup, The pharmacology of tacrine at N-methyl-D-aspartate receptors, *Prog. Neuro-Psychopharmacol. Biol. Psychiatry* 75 (2017) 54–62.
- [15] M. Kaniakova, L. Kleteckova, K. Lichnerova, K. Holubova, K. Skrenkova, M. Korinek, J. Krusek, T. Smejkalova, J. Korabecny, K. Vales, O. Soukup, M. Horak, 7-Methoxyderivative of tacrine is a 'foot-in-the-door' open-channel blocker of GluN1/GluN2 and GluN1/GluN3 NMDA receptors with neuroprotective activity in vivo, *Neuropharmacology* 140 (2018) 217–232.
- [16] E.S. Vizi, M. Kisfalvi, T. Lőrincz, Role of nonsynaptic GluN2B-containing NMDA receptors in excitotoxicity: evidence that fluoxetine selectively inhibits these receptors and may have neuroprotective effects, *Brain Res. Bull.* 93 (2013) 32–38.
- [17] M.C. Regan, Z. Zhu, H. Yuan, S.J. Myers, D.S. Menaldino, Y.A. Tahirovic, D.C. Liotta, S.F. Traynelis, H. Furukawa, Structural elements of a pH-sensitive inhibitor binding site in NMDA receptors, *Nat. Commun.* 10 (2019) 321.
- [18] H. Chaffey, P.L. Chazot, NMDA receptor subtypes: structure, function and therapeutics, *Curr. Anaesth. Crit. Care* 19 (2008) 183–201.
- [19] C.A. Lipinski, F. Lombardo, B.W. Dominy, P.J. Feeney, Experimental and computational approaches to estimate solubility and permeability in drug discovery and development settings, *Adv. Drug Deliv. Rev.* 23 (1997) 3–25.
- [20] M. Gupta, H.J. Lee, C.J. Barden, D.F. Weaver, The blood-brain barrier (BBB) score, *J. Med. Chem.* 62 (2019) 9824–9836.
- [21] F.J. Pérez-Areales, A.L. Turcu, M. Barniol-Xicota, C. Pont, D. Pivetta, A. Espargaró, M. Bartolini, A. De Simone, V. Andrisano, B. Pérez, A novel class of multitarget anti-Alzheimer benzohomoadamantane-chlorotacrine hybrids modulating cholinesterases and glutamate NMDA receptors, *Eur. J. Med. Chem.* 180 (2019) 613–626.
- [22] C. Saturnino, D. Iacopetta, M.S. Sinicropi, C. Rosano, A. Caruso, A. Caporale, N. Marra, B. Marengo, M.A. Pronzato, O.I. Parisi, N-alkyl carbazole derivatives as new tools for Alzheimer's disease: preliminary studies, *Molecules* 19 (2014) 9307–9317.
- [23] G. Marotta, F. Basagni, M. Rosini, A. Minarini, Memantine derivatives as multitarget agents in Alzheimer's disease, *Molecules* 25 (2020) 4005.
- [24] J. Patocka, D. Jun, K. Kuca, Possible role of hydroxylated metabolites of tacrine in drug toxicity and therapy of Alzheimer's disease, *Curr. Drug Metabol.* 9 (2008) 332–335.
- [25] M. Recanatini, A. Cavalli, F. Belluti, L. Piazzi, A. Rampa, A. Bisi, S. Gobbi, P. Valenti, V. Andrisano, M. Bartolini, SAR of 9-amino-1, 2, 3, 4-tetrahydroacridine-based acetylcholinesterase inhibitors: synthesis, enzyme inhibitory activity, QSAR, and structure-based CoMFA of tacrine analogues, *J. Med. Chem.* 43 (2000) 2007–2018.
- [26] D. dos Santos Pisoni, J.S. da Costa, D. Gamba, C.L. Petzhold, A.C. de Amorim Borges, M.A. Ceschi, P. Lunardi, C.A.S. Gonçalves, Synthesis and AChE inhibitory activity of new chiral tetrahydroacridine analogues from terpenic cyclanones, *Eur. J. Med. Chem.* 45 (2010) 526–535.
- [27] K.Y. Wong, A.G. Mercader, L.M. Saavedra, B. Honarparvar, G.P. Romanelli, P.R. Duchowicz, QSAR analysis on tacrine-related acetylcholinesterase inhibitors, *J. Biomed. Sci.* 21 (2014) 84.
- [28] M. Jung, J. Tak, Y. Lee, Y. Jung, Quantitative structure–activity relationship (QSAR) of tacrine derivatives against acetylcholinesterase (AChE) activity using variable selections, *Bioorg. Med. Chem. Lett.* 17 (2007) 1082–1090.
- [29] H. Boulebd, L. Ismaili, H. Martin, A. Bonet, M. Chioua, J. Marco Contelles, A. Belfaitah, New (benz) imidazopyridino tacrines as nonhepatotoxic, cholinesterase inhibitors for Alzheimer disease, *Future Med. Chem.* 9 (2017) 723–729.
- [30] L. Gorecki, L. Junova, T. Kucera, V. Hepnarova, L. Prchal, T. Kobrlova, L. Muckova, O. Soukup, J. Korabecny, Tacroximes: novel unique compounds for the recovery of organophosphorus-inhibited acetylcholinesterase, *Future Med. Chem.* 11 (2019) 2625–2634.
- [31] G.L. Ellman, K.D. Courtney, V. Andres, R.M. Featherstone, A new and rapid colorimetric determination of acetylcholinesterase activity, *Biochem. Pharmacol.* 7 (1961) 88. &.
- [32] N.H. Greig, D.K. Lahiri, K. Sambamurti, Butyrylcholinesterase: an important new target in Alzheimer's disease therapy, *Int. Psychogeriatr.* 14 (2002) 77.
- [33] O. Lockridge, Review of human butyrylcholinesterase structure, function, genetic variants, history of use in the clinic, and potential therapeutic uses, *Pharmacol. Ther.* 148 (2015) 34–46.

- [34] J. Korabecny, K. Musilek, O. Holas, J. Binder, F. Zemek, J. Marek, M. Pohanka, V. Opletalova, V. Dohnal, K. Kuca, Synthesis and in vitro evaluation of N-alkyl-7-methoxytacrine hydrochlorides as potential cholinesterase inhibitors in Alzheimer disease, *Bioorg. Med. Chem. Lett* 20 (2010) 6093–6095.
- [35] S.F. Traynelis, L.P. Wollmuth, C.J. McBain, F.S. Menniti, K.M. Vance, K.K. Ogden, K.B. Hansen, H. Yuan, S.J. Myers, R. Dingledine, Glutamate receptor ion channels: structure, regulation, and function, *Pharmacol. Rev.* 62 (2010) 405–496.
- [36] J. Konecny, A. Misiachna, M. Hrabanova, L. Pulkrabkova, M. Benkova, L. Prchal, T. Kucera, T. Kobrlova, V. Finger, M. Kolcheva, Pursuing the complexity of alzheimer's disease: discovery of fluoren-9-amines as selective butyrylcholinesterase inhibitors and N-Methyl-D-Aspartate receptor antagonists, *Biomolecules* 11 (2021) 3.
- [37] H. Moriawaki, Y.-S. Tian, N. Kawashita, T. Takagi, Mordred: a molecular descriptor calculator, *J. Cheminf.* 10 (2018) 4.
- [38] P. Paoletti, C. Bellone, Q. Zhou, NMDA receptor subunit diversity: impact on receptor properties, synaptic plasticity and disease, *Nat. Rev. Neurosci.* 14 (2013) 383–400.
- [39] O. Soukup, J. Korabecny, D. Malinak, E. Nepovimova, N. Pham, K. Musilek, M. Hrabanova, V. Hepnarova, R. Dolezal, P. Pavek, In Vitro and in Silico Evaluation of Non-quaternary Reactivators of AChE as Antidotes of Organophosphorus Poisoning-A New Hope or a Blind Alley?, *Medicinal Chemistry, Shariqah (United Arab Emirates)*, 2018.
- [40] P. Garberg, M. Ball, N. Borg, R. Cecchelli, L. Fenart, R. Hurst, T. Lindmark, A. Mabondzo, J. Nilsson, Q. Raub, In vitro models for the blood–brain barrier, *Toxicol. Vitro* 19 (2005) 299–334.
- [41] J. Zdarova Karasova, O. Soukup, J. Korabecny, M. Hroch, M. Krejciova, M. Hrabanova, J. Misik, L. Novotny, V. Hepnarova, K. Kuca, Tacrine and its 7-methoxy derivative; time-change concentration in plasma and brain tissue and basic toxicological profile in rats, *Drug Chem. Toxicol.* (2019) 1–8.
- [42] W.P. McNally, W.F. Pool, M.W. Sinz, P. Dehart, D.F. Ortwine, C.C. Huang, T. Chang, T.F. Woolf, Distribution of tacrine and metabolites in rat brain and plasma after single- and multiple-dose regimens. Evidence for accumulation of tacrine in brain tissue, *Drug Metabol. Dispos.* 24 (1996) 628–633.
- [43] J. Grotta, W. Clark, B. Coull, L.C. Pettigrew, B. Mackay, L.B. Goldstein, I. Meissner, D. Murphy, L. LaRue, Safety and tolerability of the glutamate antagonist CGS 19755 (selfotel) in patients with acute ischemic stroke: results of a phase IIa randomized trial, *Stroke* 26 (1995) 602–605.
- [44] J.H. Krystal, L.P. Karper, J.P. Seibyl, G.K. Freeman, R. Delaney, J.D. Bremner, G.R. Heninger, M.B. Bowers, D.S. Charney, Subanesthetic effects of the noncompetitive NMDA antagonist, ketamine, in humans: psychotomimetic, perceptual, cognitive, and neuroendocrine responses, *Arch. Gen. Psychiatr.* 51 (1994) 199–214.
- [45] K.W. Muir, K.R. Lees, Clinical experience with excitatory amino acid antagonist drugs, *Stroke* 26 (1995) 503–513.
- [46] T. Bast, W. Zhang, J. Feldon, I.M. White, Effects of MK801 and neuroleptics on prepulse inhibition: re-examination in two strains of rats, *Pharmacol. Biochem. Behav.* 67 (2000) 647–658.
- [47] M. Chatterjee, S. Ganguly, M. Srivastava, G. Palit, Effect of 'chronic' versus 'acute' ketamine administration and its 'withdrawal' effect on behavioural alterations in mice: implications for experimental psychosis, *Behav. Brain Res.* 216 (2011) 247–254.
- [48] D. Manahan-Vaughan, D. von Haebler, C. Winter, G. Juckel, U. Heinemann, A single application of MK801 causes symptoms of acute psychosis, deficits in spatial memory, and impairment of synaptic plasticity in rats, *Hippocampus* 18 (2008) 125–134.
- [49] D. Carriero, G. Outslay, A. Mayorga, J. Aberman, G. Gianutsos, J.D. Salamone, Motor dysfunction produced by tacrine administration in rats, *Pharmacol. Biochem. Behav.* 58 (1997) 851–858.
- [50] J.G. Csernansky, M. Martin, R. Shah, A. Bertchume, J. Colvin, H. Dong, Cholinesterase inhibitors ameliorate behavioral deficits induced by MK-801 in mice, *Neuropsychopharmacology* 30 (2005) 2135.
- [51] S.-Y. Pan, Z.-L. Yu, C.-J. Xiang, H. Dong, H.-Y. Fang, K.-M. Ko, Comparison studies of tacrine and bis (7)-tacrine on the suppression of scopolamine-induced behavioral changes and inhibition of acetylcholinesterase in mice, *Pharmacology* 83 (2009) 294–300.
- [52] H. Wang, P.R. Carlier, W.L. Ho, D.C. Wu, N.T.K. Lee, C.P. Li, Y.P. Pang, Y.F. Han, Effects of bis (7)-tacrine, a novel anti-Alzheimer's agent, on rat brain AChE, *Neuroreport* 10 (1999) 789–793.
- [53] D.R. Liston, J.A. Nielsen, A. Villalobos, D. Chapin, S.B. Jones, S.T. Hubbard, I.A. Shalaby, A. Ramirez, D. Nason, W.F. White, Pharmacology of selective acetylcholinesterase inhibitors: implications for use in Alzheimer's disease, *Eur. J. Pharmacol.* 486 (2004) 9–17.
- [54] K. Chalupova, J. Korabecny, M. Bartolini, B. Monti, D. Lamba, R. Caliendo, A. Pesaresi, X. Brazzolotto, A.J. Gastellier, F. Nachon, J. Pejchal, M. Jarosova, V. Hepnarova, D. Jun, M. Hrabanova, R. Dolezal, J.Z. Karasova, M. Mzik, Z. Kristofikova, J. Misik, L. Muckova, P. Jost, O. Soukup, M. Benkova, V. Setnicka, L. Habartova, M. Chvojikova, L. Kleteckova, K. Vales, E. Mezeiova, E. Uliassi, M. Valis, E. Nepovimova, M.L. Bolognesi, K. Kuca, Novel tacrine-tryptophan hybrids: multi-target directed ligands as potential treatment for Alzheimer's disease, *Eur. J. Med. Chem.* 168 (2019) 491–514.
- [55] K. Skrenkova, J.-m. Song, S. Kortus, M. Kolcheva, J. Netolicky, K. Hemelikova, M. Kaniakova, B.H. Krausova, T. Kucera, J. Korabecny, The pathogenic S688Y mutation in the ligand-binding domain of the GluN1 subunit regulates the properties of NMDA receptors, *Sci. Rep.* 10 (2020) 1–15.
- [56] M. Kaniakova, K. Lichnerova, L. Vyklicky, M. Horak, Single amino acid residue in the M4 domain of GluN1 subunit regulates the surface delivery of NMDA receptors, *J. Neurochem.* 123 (2012) 385–395.
- [57] M. Kaniakova, J. Korabecny, K. Holubova, L. Kleteckova, M. Chvojikova, K. Hakenova, L. Prchal, M. Novak, R. Dolezal, V. Hepnarova, 7-phenoxytacrine is a dually acting drug with neuroprotective efficacy in vivo, *Biochem. Pharmacol.* (2021) 114460.
- [58] A. Höskuldsson, PLS regression methods, *J. Chemom.* 2 (1988) 211–228.
- [59] S. Wold, E. Johansson, M. Cocchi, PLS: Partial Least Squares Projections to Latent Structures, 1993.
- [60] S. Wold, W.J. Dunn III, Multivariate quantitative structure-activity relationships (QSAR): conditions for their applicability, *J. Chem. Inf. Comput. Sci.* 23 (1983) 6–13.
- [61] S. Wold, Validation of QSAR's, *Quant. Struct.-Act. Relat.* 10 (1991) 191–193.
- [62] J.Z. Karasova, V. Hepnarova, R. Andrys, M. Lisa, P. Jost, L. Muckova, J. Pejchal, D. Herman, D. Jun, J. Kassa, Encapsulation of oxime K027 into cucurbit [7] uril: in vivo evaluation of safety, absorption, brain distribution and reactivation effectiveness, *Toxicol. Lett.* 320 (2020) 64–72.